THESIS

DISRUPTIVE PACKING OF BINARY MIXTURE

Submitted by

Shuai Zou

Department of Civil and Environmental Engineering

In partial fulfillment of the requirements

For the Degree of Master of Science

Colorado State University

Fort Collins, Colorado

Summer 2016

Master's Committee:

Advisor: Paul Heyliger

Christopher Bareither
Scott Shuler

ABSTRACT

DISRUPTIVE PACKING OF BINARY MIXTURES

Granular materials are common in many areas such as civil engineering, food industry, and chemistry. The discrete element method has been demonstrated to be an effective method to study the particle dynamics of such materials over the past several decades. The packing of monosized spherical particles has been well studied from both numerical and experimental perspectives. However, the study of packings of a binary mixture that contains particles of two different sizes has been limited because of the numerous variables that affect the packing structure.

The potential variables for packing of binary mixtures of spherical particles blended by geometric disruptors in a gravity loaded ramp are evaluated in this thesis. The complexity of the disruptor geometry was used as the primary variable to study the resulting packing of two different-sized particles. The final packing structure was quantified by coordination number, radial distribution function, packing density, and vertical position of the smaller-diameter particles. Based on the analysis conducted in this thesis, the mean coordination number of all particles, larger particles and smaller particles, generally increases with the complexity of disruptor geometry. The mean vertical position of smaller particles decrease with an increase in the complexity of the disruptor geometry. The radial distribution function of each type of particle in a binary mixture has the same characteristics of the radial distribution function of mono-size particle packing. The methodology presented in this thesis can be effective to analyze binary mixtures of spherical particles.

ACKNOWLEDGEMENTS

I would first like to thank my thesis advisor Dr. Heyliger of the Department of Civil Engineering at Colorado State University. The door to Prof. Heyliger office was always open whenever I ran into a trouble spot or had a question about my research or writing. He consistently allowed this paper to be my own work but steered me in the right the direction whenever he thought I needed it.

I would also like to acknowledge Dr. Bareither of the Department of Civil Engineering at Colorado State University as the second reader of this thesis, and I am gratefully indebted to him for his very valuable comments on this thesis.

Finally, I must express my very profound gratitude to my parents for providing me with unfailing support and continuous encouragement throughout my years of study and through the process of researching and writing this thesis. This accomplishment would not have been possible without them. Thank you.

TABLE OF CONTENTS

LIST OF TABLES

LIST OF FIGURES

1 OVERVIEW AND THEORY

Granular materials are probably one of the most common materials encountered in nature, and for this reason research on the mechanics of granular materials can be found in many different science and engineering fields. Aggregates used in civil construction are generally in granular form and their engineering properties depend on the physical characteristics of the individual grains and the way these grains interact with one another. The packing of granular material is a rapidly developing interdisciplinary research area in civil engineering. some definitions of terms used in this thesis are explained: (1) packing density (1-void ratio): the fraction of the space filled by the figures making up the packing. (2) coordination number: the number of contacts on the particle. (3) The radial distribution function g(r): the probability distribution of finding the center of a particle in a given position at distance r from a reference point.

The discrete element method (DEM) is a numerical method that can simulate the motion of assemblies of particles. The differential equations governing particle the motion of the particles are used to determine particle movement position and following each time step of a model simulation. Duran (2012) [4] and Zhu (2007) [2] divide the numerical techniques used in DEM into two main categories: (1) soft sphere models and (2) hard sphere models. The major difference between the two models is whether penetration is allowed at particle contacts. Both types of simulation are transient, or time dependent. This means that the assembly of particles is updated or examined following each time interval, whereas the global assessment of the entire aggregate system is considered over a much longer time period.

The hard sphere model is based on so called collisional or event driven models (ED model). In this type of model, inter-particle penetration or deformation is ignored during the process of impact between adjacent particles. The ED model is governed by momentum exchange equations. The particle contact force, which is the major tool of the soft sphere model, is not clearly stated in the ED model. The resultant loss of momentum caused by a collision between particles is only determined by means of the coefficients of elastic restitution

since the dissipated energy is related to plastic deformation and heat when particles impact. Coefficients of elastic restitution are specified in two orthotropic directions, typically the normal and tangential.

The ED model also has some drawbacks. Details of the response of dense granular material are nearly impossible to capture. The ED model is used to simulate multiple simultaneous contacts on a single particle. Additionally, the ED model lacks the ability to represent tangential or frictional forces accurately between two interacting particles of a system.

Soft sphere models also solve the governing equations of motion within an appropriate time step, but allow interacting particles to overlap at contact points. The goal of allowing overlap is to simulate the normal and tangential components of the inter-particle force and deformation at the contact point. The advantage of the soft sphere approach is that multiple simultaneous contacts are allowed within one discrete time increment.

The distinct element method as used in this thesis was first developed by Cundall and Strack (1979a) [5]. According to the definitions of the soft and hard sphere approaches, the distinct element method belongs to the soft sphere model approach. The two essential conditions in DEM are particle coordinates and boundary conditions. Material properties are also important in DEM analyses, but the input parameters are varied depending on the contact force model. More details of the contact force model are provided in the following chapters.

1.1 Framework of DEM

The general solution path of DEM analyses includes two differential equations that are solved each time step. First, particle velocities and incremental displacements are updated by enforcing dynamic equilibrium for each particle. Second, contact forces are calculated based on particle velocities and incremental displacements. In most cases, the contact force consists of two orthogonal components, which are the tangential component and normal component. Tangential components usually cause rotations of individual particles. The

normal components of the contact force can also induce moments on non-spherical (3D) or non-disk (2D) particles. Lastly, the forces and moments generated from the two orthogonal force components are used to update particle positions in the next time step by solving the governing equations of motion. Generally speaking, such problems can be solved in time by an implicit and explicit approach. Implicit approaches are very similar to those used in matrix structural analysis and the finite element method (FEM). Each individual particle in the DEM system can be treated as end points of the structural element or the nodes in FEM. The differential equation of individual particles can be written as,

$$M\ddot{u} + C\dot{u} + K(u) = \triangle F \tag{1}$$

where M is the mass matrix, C is a damping matrix, u is the incremental displacement vector (3 displacement and 3 rotation), there are 6 DOF per particle in 3D and 3 DOF in 2D. F is the incremental force and moment vector, and K is the global stiffness matrix. Finding u is the goal of all DEM analysis.

Implicit approaches include large numbers of global stiffness matrices for all particles in the system when assembly of each particle is modeled. This makes implicit approach computational expensive compared to explicit approach due to : (1) obtain the global stiffness matrix, the transform matrix of all interacting particles should be calculated, and (2) the stiffness matrix varies with each particle.

The explicit approach was first proposed by Cundall and Strack (1979a, b) [5] [6] and is much less computationally intensive compared to the implicit method since the global stiffness matrix does not need to be calculated. The governing equations for each particle are given as,

$$m_i \frac{d\vec{v_i}}{dt} = f_{pf,i} + \sum_{j=1}^{k_c} (f_{c,ij} + f_{d,ij}) + m_i g \tag{2}$$

$$I_i \frac{d\vec{w}_i}{dt} = \sum_{j=1}^{k_c} (M_{t,ij} + M_{r,ij}) \tag{3}$$

where v_i and w_i are, respectively, the translational and angular velocities of the particle, k_c is the number of particles in interaction with the particle, $f_{pf,i}$ is the particle-fluid interaction force, and $f_{c,ij}$ and $f_{d,ij}$ are the inter-particle forces between particle which are, the elastic force and viscous damping force respectively. In this equation, $f_{c,ij}$ and $f_{d,ij}$ are the contact forces between particles caused by deformation of the particles.

According to Zhu (2007) [2], a more accurate system of governing equation is

$$m_i \frac{d\vec{v}_i}{dt} = F_i^f + \sum_j F_{ik}^{nc} + \sum_k F_{ik}^c + F_i^g, \tag{4}$$

and

$$I_i \frac{d\vec{w}_i}{dt} = \sum_j M_{ij} \tag{5}$$

Eq.4 includes the term F_{ik}^{nc}, which is the non-contact force acting on particle by particle k or other sources. Typically, the non-contact forces involve a combination of three fundamental forces, which include van der Waals , electrostatic and capillary forces. The van der Waals force is calculated by the Hamker theory (Hamaker, 1937 [7] and Israelachvili, 2011 [8]):

$$F^v = -\frac{Ad_p}{24h^2} n_{ij} \tag{6}$$

Where d_p is the diameter of particles, h is the distance between the particles, A is called the interaction constant (i.e. Hamker constant), n_{ij} is the direction vector between ith particle and jth particle.

The electrostatic force exists between charged particles and can be classified as one of three types: Coulombic forces, image-charge forces, and space-charge forces. The classical Coulomb equation is usually used to approximate the electrostatic force:

$$F^e = -\frac{Q^2}{16\pi q_0 h^2}(1 - \frac{h}{\sqrt{(R^2 + h^2)}})n_{ij} \tag{7}$$

where R is the radius of particle, h is the distance between particles, q_0 is permittivity of empty space, Q is the point charge, n_{ij} is the direction vector between ith particle and jth particle.

The capillary force is caused by surface tension at the solid/liquid/gas interfaces and is the force due to the reduced hydrostatic pressure in the bridge. Capillary force can be calculated as

$$F^l = 2\pi\gamma R sin\phi sin(\phi + \theta) + \Pi R^2 \Delta p sin^2\phi \tag{8}$$

where γ is the liquid surface tension, ϕ is the half-filling angle, θ is the contact angle, and Δp can be calculated by the Laplace-Young equation.

The F term in Eq.4 can be determined by the acceleration from differential equation of linear motion. If the translational motion is uncoupled from the rotational motion, the differential equation of linear motion is given as,

$$m_p a_p^t = F_p^t \tag{9}$$

where m_p is the mass matrix, a^t is the acceleration vector at time t, and F_p^t is the F term from Eq.4. The acceleration and velocity of individual particles found from Eq.9 mentioned above can be used to update the particle positions.

1.2 Time integration method

The time integration method is important for tracking particle position. The definition of time integration method is the method used to get any parameter (typical position) when the parameters first or second derivatives with respect to time are known. In the present case, it is the method used to calculate the displacements of each individual particle using acceleration and velocity found from previous time steps. The most common time integration approach for translational motion is the central difference method, given as

$$a_p^t = \frac{1}{\triangle t}(v^{t+\triangle t/2} - v_p^{t-\triangle t/2}) \tag{10}$$

where $v^{t+\triangle t/2}$ and $v_p^{t-\triangle t/2}$ are the velocity vectors at $t + \triangle t/2$ and $t - \triangle t/2$ and respectively for particle p.

The most common time integration approach for rotation is

$$w_{p,z}^{t+\triangle t/2} = w_{p,z}^{t-\triangle t/2} + \triangle t \frac{M_{p,z}^t}{I_{p,z}} \tag{11}$$

where $w_{p,z}$ is the angular velocity about an axis through the centre of the particle orthogonal to the analysis plane, $M_{p,z}$ is the moment of the particle, and $I_{p,z}$ is the moment of inertia of the particle. Both approaches were used in the present study.

1.3 Contact forces

Contact forces between impacting particles are significant in DEM analysis. Sutmann (2002) [9] estimates that 90 percent of the computational time used in DEM simulations is the calculation related to contact forces. The strategy to calculate contact forces becomes important to reduce simulation time. In reality, the contact between two compacting particles is complex since particle geometry, material properties, and particle motion each have a large influence on the distribution of the contact stress. In reality, there are two stages of particle

contact. The first stage is contact that occurs at asperities on the surface of particle. The second stage is when two particles contact over a finite area after the asperities deform and yield. To simplify calculation of the contact force, most DEM models use single points as contacts and assume the particle surface is smooth.

Contact forces in DEM are a very significant issue since they are used to simulate wall-particle interaction and particle-particle interaction. They can be resolved into two orthogonal components: normal and tangential to the contact point. Contact constitutive models based on a combination of spring sliders and dashpots are used to simulate the stress-deformation response that occur at contact points. Many different contact constitutive models have been discussed by different researchers.

In contact mechanics, there are two kinds of contacts: conforming and non-conforming. These are shown in Figure 1. Non-conforming contacts are those that occur when two compacting particles meet at single contact point at the beginning of the contact process. The stress from contact is concentrated at a contact zone which is very small. The conforming contact is more complex, since the contact location is more than one point due to the morphology of the two compacting surface. The distribution of stress becomes highly complex since multiple contact points exist. In actuality, the contact of the particle should be modeled as the combination of conforming and non-conforming contacts due to the presence of surface asperities. The most likely contacting process of two actual particles is that the initial contact is a combination of conforming and non-conforming contacts, then the contact becomes purely conforming assuming the surface asperities yield. In the majority of DEM codes, spheres are used to model the particles since contacts between two spheres are non-conforming. This is the simplest way to model contact and greatly simplifies the analysis. Many researchers are working on non-spherical DEM codes, but the accuracy of the contacting process is still under investigation.

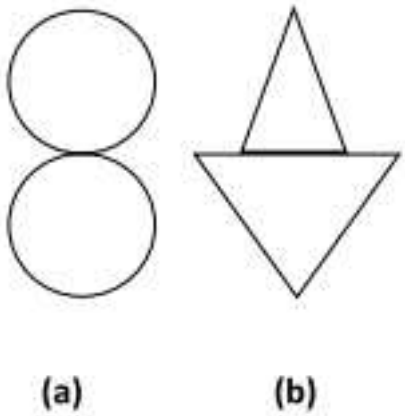

Figure 1: Contact types: (a) non-conforming contact and (b) conforming contact

Elastic normal response

Hertizan contact mechanics are used to calculate the normal responses between particles. Hertz (1882) [10] developed a contact mechanics theory giving an expression of load-deformation response when non-conforming contact occurs between two particles. The deformation at the contact point is

$$\delta = (\frac{9F_n^2}{16R^*E^{*2}})^{1/3} \tag{12}$$

where F_n is the applied load, R^* is effective particle radius, and E^* is effective Young's modulus.

Linear spring-dashpot model

The spring-dashpot model proposed by Cundall and Strack (1979) [5] is the most commonly used linear model in DEM codes due to its simplicity. The equations for normal contact force (f_n) and tangential contact force (f_t) for spherical particles are given as,

$$f_n = -K_n\delta_n n_c - C_n(v_c \cdot n_c)n_c \tag{13}$$

$$f_t = -K_t v_c^t + C_t(v_c \times n_c) \times n_c \tag{14}$$

where δ_n is the normal response, C_n and C_t are the damping ratio in normal and tangential direction, respectively, and K_n and K_t are stiffness in the normal and tangential directions, respectively.

The linear spring model without a dashpot that represents the viscous dissipation is also used by many researchers. Latzel (2000) [11] claims that the linear spring model is sufficient

for most 2D DEM models. The spring stiffness in this model can not be directly related to material properties, but is usually determined experimently to match the response of particles to an effective spring constant.

Simplified Hertizan-Mindlin and Deresiewicz contact model

A model based on Hertizan-Mindlin and Deresiewicz contact model was proposed by Langston (1994) [12]. Mindlin and Deresiewicz (1953) [13] modified the Hertz theory to derive the force- displacement relationship in the tangential direction. Unfortunately, the Hertizan-Mindlin contact model is time-consuming. Many researchers use a a simplified Hertizan-Mindlin and Deresiewicz contact model, whereby f_n and f_t are computed as

$$f_n = -\frac{4}{3}E^*\sqrt{R^*}(\delta_n^{3/2}n_c - C_n(8m^*E^*\sqrt{R^*\delta_n})^{1/2} \cdot (v_c * n_c)n_c \tag{15}$$

$$f_t = -\mu|f_{n,e}|(1-(1-|v_c^t|/\delta_{max})^{3/2})v_c^t + 2C_t(1.5\mu m * |f_{n,e}| \cdot \sqrt{1-|v_c^t|/\delta_{max}}/\delta_{max})^{1/2} \cdot (v_c \times n_c) \times n_c \tag{16}$$

where R^* is effective particle radius, E^* is effective Young's modulus. δ_n is normal response, C_n and C_t are the damping ratio in normal and tangential direction,respectively, m^* is the effective mass, μ is coefficient of kinetic friction.

Walton-braun linear model

Walton and Braun (1986) [14] suggest that the normal contact force can be calculated from a semi-latched spring force-displacement model in the normal direction and an approximation of the Mindlin and Deresiewicz contact theory could be used to calculate the tangential force. The formula for the normal force is shown below,

$$f_n = \begin{cases} -k_1 \delta_n n_c, \dot{\delta_n} \geq 0 & (loading) \\ -k_2(\delta_n - \delta_{n0}) n_c, \delta_n < 0 & (unloading) \end{cases}$$

2 LITERATURE REVIEW

Discrete particle simulations are widely used in industry, and an example of this is the mixing of two different sized particles, as considered in this work. Selecting a method of simulating particle dynamics is something of a challenge. To optimize practical methods that can be used in engineering practice, an assessment of candidates by both numerical simulation and laboratory mixing is essential. Various mixing devices could be tested in laboratory, but the vast array of possible choices can soon overwhelm practical considerations. Numerical models provide a useful alternative so that 1) the number of physical experiments can be reduced, and 2) the internal structure of the deposited constituents can be visualized and quantified. An important numerical method, called the discrete element method (DEM) can be used to simulate such mixing.

In past two decades, DEM have been developed to address different engineering challenges by many researchers. Tsuji (1993) [15] and Xu (1997) [16] mentioned the method used to couple DEM with computational fluid dynamics can simulate particle-fluid flow. In this work, however, the analysis is confined to mixing of dry particles.

2.1 Particle packing: The general case

Diverse methods have been developed to quantify the structure of particle packing. These methods can be used to quantify engineering properties such as effective thermal conductivity or pore connectivity. Coordination number and radial distribution function are particle packing parameters that can be used to relate to engineering properties of granular media.

2.1.1 Packing of cohesionless particles

There are various ways to form a packing of particles. Many researchers have done various DEM studies such as pouring or depositing particles under gravity (Yen and Chaki, 1992; Zhang et al., 2001; Latham et al., 2001; Silbert et al., 2002a,b; Bertrand et al., 2004; Latham

and Munjiza, 2004; Munjiza and Latham, 2004; An et al., 2005), centripetal growth (Liu et al., 1999; Liu and Yuan, 2000), compression (Liu, 2003; Luding, 2004; Zhang and Makse, 2005; Alonso-Marroquin et al., 2005) [17]. To compare simulated results with experimental results, macroscopic properties, microscopic structure, and force network have been discussed in numerous papers.

1. Macroscopic properties: Packing density and porosity in DEM simulations have been used to compare with values from experiment under similar conditions. These parameters are two basic values and are the easiest to obtain. In experiments of packings of monosized spheres, the random loose packing (RLP) and random close packing (RCP) are the two most well known packing states.The RLP is the loosest particle packing possible that corresponds to the largest amount of void space between particles, whereas the RCP is the closest particle packing and smallest amount of void space between particles. The measured packing densities of these two states are 0.59 (RLP) and 0.64 (RCP). The range of packing density in DEM simulation is from 0.55 (RLP) to 0.645 (RCP) (Yen and Chaki, 1992; Zhang and Makse, 2005). The value match random loose packing (RLP) and random close packing (RCP).

2. Microstructural properties: coordination number and radical distribution function are common and straightforward parameters in DEM. They are used to quantify the structure of particle packing. For example, Zhang (2000) mentioned that coordination number decreases with some dynamic factor for packing of monosized sphere.

3. The effect of dynamic factor: A few researchers have conducted DEM simulations to evaluate the effects of dynamic factor which is the variable affecting the packing dynamics (Zhang et al., 2001; Silbert et al., 2002a; Zhang and Makse, 2005) [17]. As shown in Figure 2, the effect of dynamic factor is associated with packing method and material property. Two mechanisms (externally supplied energy and energy dissipation rates) cause the effects (Silbert et al., 2002) [18].

The two random packing states of RLP and RCP are well known (Scott, 1960; German, 1989; Bideau and Hansen, 1993; Mehta, 1994) [17]. In experiments, RCP can be achieved by

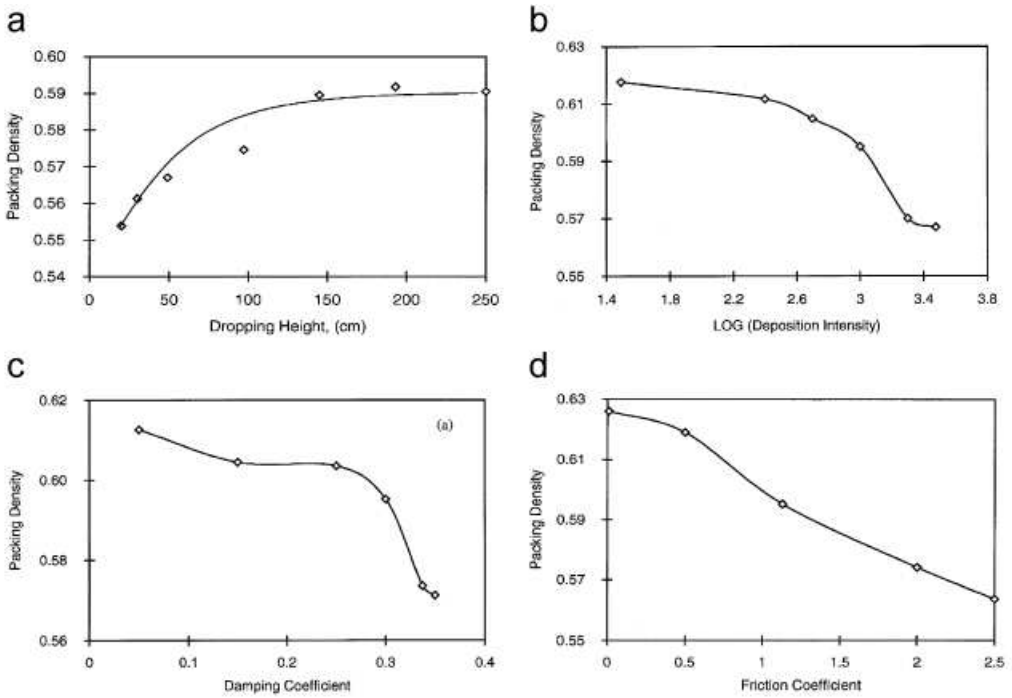

Figure 2: Packing density as a function of (a) dropping height; (b) deposition density; (c) damping coefficient; and (d) friction coefficient (Zhang et al., 2001) [1].

compaction or vibration. But the transition process from RLP to RCP cannot be visualized because lack of detail about force networks and internal structure rearrangement. An et al. (2005) [17] successfully modeled the transition from RLP to RCP by one-dimensional vibration, when vibration amplitude and frequency are the two controlled parameters. The result of numerical models shows that RCP can be achieved when these two parameters were properly controlled.

2.1.2 Packing of cohesive particles

The difference between cohesive particle and cohesionless particles is realized via a non-contact force. Cohesive particles is associate with numerous non-contact forces. The non-contact force between particles includes van der Waals force, electrostatic force and capillary force.

van der Waals forces were first proposed by Yen and Chaki (1992) [2] in DEM simulations. The results from numerical analysis did not match experimental results. Yang et al. (2000, 2002, 2003c, 2006b, 2008a,b) [2] proposed that the results from numerical simulations only matched the measured result (Milewski, 1987; Feng, 1998) [2] when the particle size is less than 1 μm. Measured and simulated results show that the packing structure varied with particle size and porosity as shown in Figure 3.

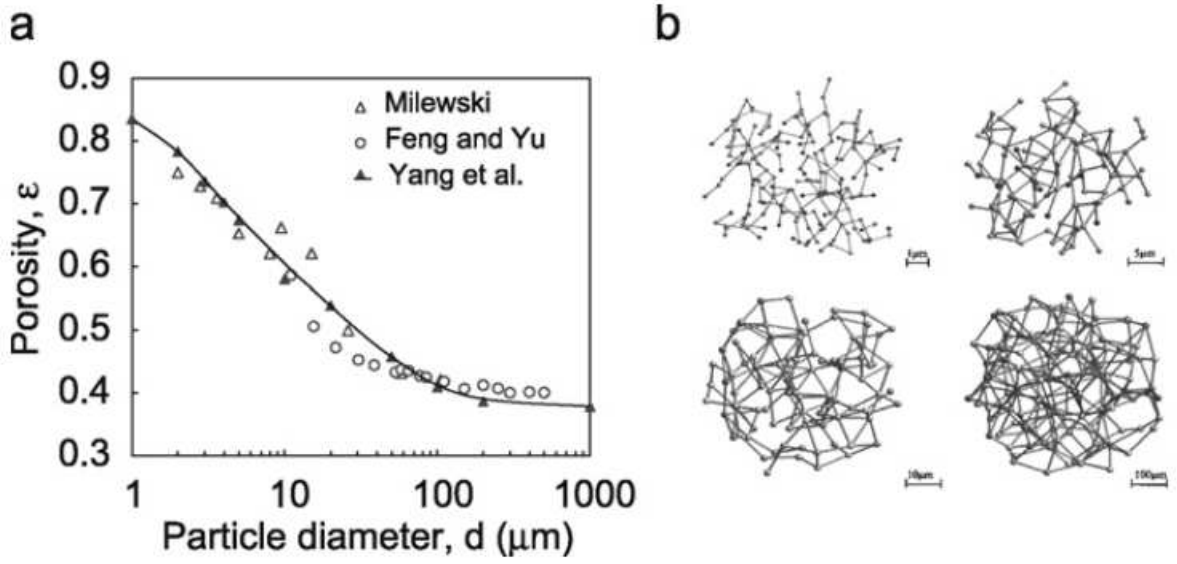

Figure 3: (a) Porosity as a function of particle size: simulated vs. measured and (b) the contact networks in a spherical sample taken from the packing of different sized particles, where small spheres represent the centres of particles, and sticks represent the contacts between particles (Yang et al., 2000) [2].

The radical distribution function (RDF) is normally used to quantify the variation of the packing structure from RLP to RCP since RDF of a dense random packing has been well established. In Figure 4, as particle size decreases, the first peak in RDF becomes narrower, with a sharp decrease to the first minimum. The first component of the second peak vanishes when particle size is less than 100 um and the peaks beyond the second one gradually vanish. The dominant force is shown to transition to van der Waals force instead of gravity when the particle diameter is less than 100 um. In other words, the RDF shows that packing of fine particles is inter-particle force dominated and packing of coarse particles

is a gravity dominated problem. Yang (2000) [17] has mentioned that radical distribution function, angular distribution, and coordination number are three effective parameters to quantify packing structure.

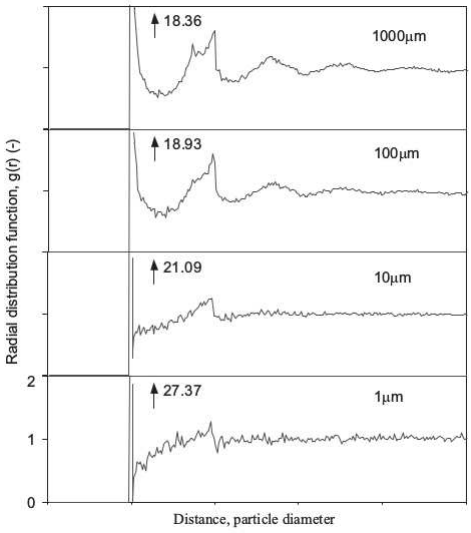

Figure 4: Radial distribution function as a function of particle size (Yang et al., 2000) [2].

3 METHODOLOGY

The purpose of this study is to determine the differences in the packing structure of a mixture of binary spheres depending on the geometric configuration of a static system used to mix the particles together. The packing of mono-size particles has been well studied and understood over the past decade, but this packing is still considered in the present work. The binary sphere mixture is less well understood in terms of numerical modeling, especially for pure mixing problems. To determine the dynamic behavior of binary sphere mixtures, numerical models were created to simulate the mixing of spherical particles with different static mixer designs.

3.1 Packing parameters of mixtures

It is difficult to tell how well a binary packing is mixed. So the coordination number, radial distribution function, and packing density are determined to quantify the final configuration of binary mixture.

3.1.1 Packing density

Packing density is an important parameter to quantify the overall packing structure. In engineering practice, the packing density often is used as either a global property or a local property. In experimental and numerical measurements, methods of measuring the packing density have been well established for mono-size particle packings. Measurements of packing density for binary sphere mixtures are more complicated at the local level since experimental measurements lack details of the final position of each particle. The global packing density is therefore usually used to quantify packing structure by experiment. In numerical simulations, the local packing density is easier to obtain than experiment since the final position of all particles are calculated numerically. The formula of the global packing density is given as,

$$\rho = \frac{NV_{particles}}{V} \tag{17}$$

Where N is the number of the particles, $V_{particles}$ is the volume of each particle, and V is the volume occupied by all the particles (control volume).

3.1.2 Local packing density

The local packing density is a straightforward parameter that can be used to quantify microstructure of granular media. The spatial distribution of the local packing density can be used to analyze mixtures and wall effects of the container. Different methods of calculating the local packing density have been developed. For mono-size particle packings, Voronoi tessellation is known to be an effective tool. As shown in Figure 5, the packing system of multiple mono-size spheres can be divided by Voronoi cells. The Voronoi cell belonging to one particular sphere (a) is defined as the total of the space's points that are closer to its center than to the center of any other sphere within the system. The 3D example of Voronoi cell is shown in Figure 6.

As shown in Figure 7 from Riccardo (2008) [19] for a binary sphere mixture, Voronoi tessellation is not an appropriate method to calculate the local packing density of bidisperse assemblies of spheres since large particles can be cut by separation planes, meaning that local packing densities of large particles are not able to be calculated accurately. Other methods mentioned by Annic (1994) [19] had been developed to calculate the local density of ploydisperse assemblies of spheres, which include the radical tessellation (Annic et al 1994) [19] and the navigation map. Radical tessellations are those in which the radical plane, consisting of the points with equal tangent relative to the two spheres are used as the separation plane. The navigation map can be formed when the pieces of a hyperboloid is built that consists of the sets of points equidistant from the surface of the spheres. Both

Radical tessellation and navigation map are the same as the Voronoi tessellation for mono-sized spheres. Details of three methods are shown in Figure 7. The formula used to calculate the local packing density (ρ) is given as,

$$\rho = \frac{V_{particle}}{V} \tag{18}$$

where $V_{particle}$ is the volume of a single particle, and V is the volume of Voronoi tessellation for mono-size packing, or the volume of Radical tessellation or Navigation map for a binary mixture.

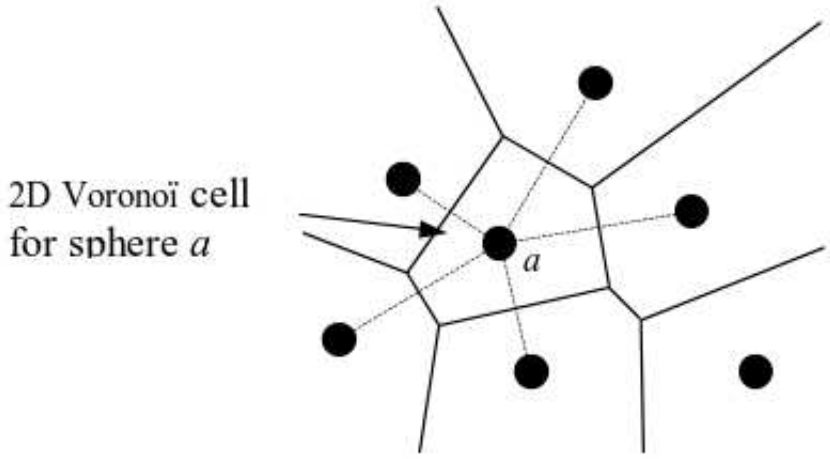

Figure 5: 2D example of Voronol tessellation

3.1.3 Radial distribution function

Radial distribution function is used to characterize the packing structure from numerical perspective. The formula used to calculate this function for spheres is given by,

$$g(r) = \frac{V}{N}\frac{\mathrm{d}N(r)}{4\pi r^2 \mathrm{d}r} \tag{19}$$

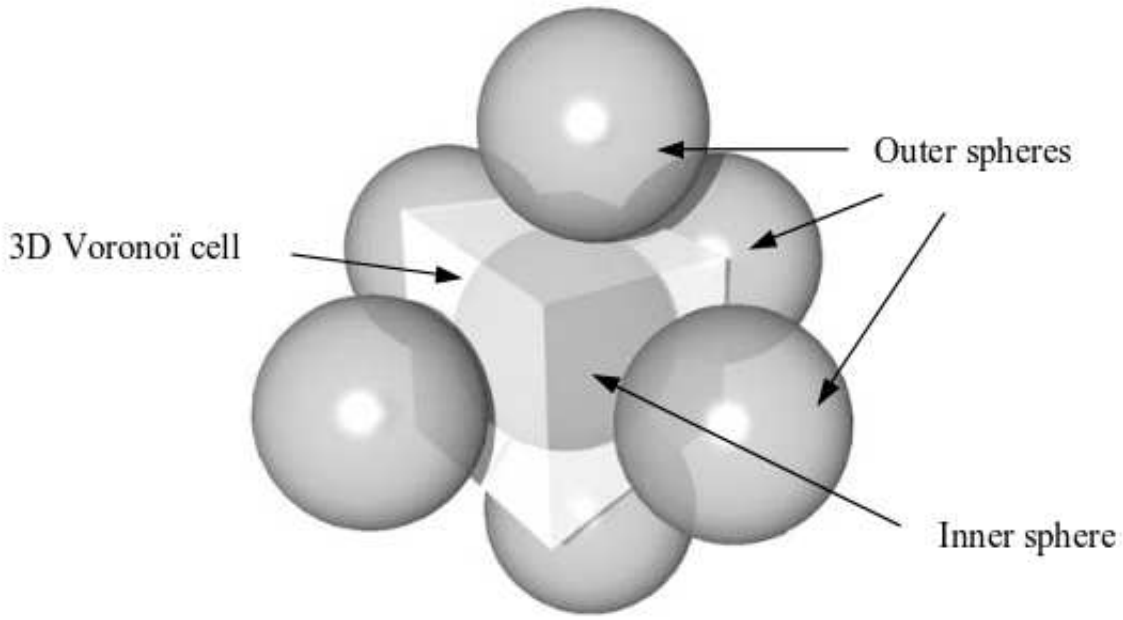

Figure 6: 3D example of Voronol cell

where V represents the total volume of the hexahedron that all particles occupy, N is the total number of particles and $dN(r)$ is the number of particles in a shell of width dr at distance r from the reference particle.

The radial distribution function for mono-size packings have been found by experiment and also by numerical simulations. Two sharp peaks are usually observed in this function, there is a first sharp peak located at one particle diameter as measured from any arbitrary point in packing, and a second peak that for mono-size packing varies with packing structure. For dense packing, the second peak splits into two peaks which develop at $\sqrt{3}d$ and $2d$, and the first splitting will vanish as the packing becomes less dense. It is essential to have a basic understanding of the relationship between the two peaks and the local configuration. More details are illustrated in Figures 8, 9 and 10.

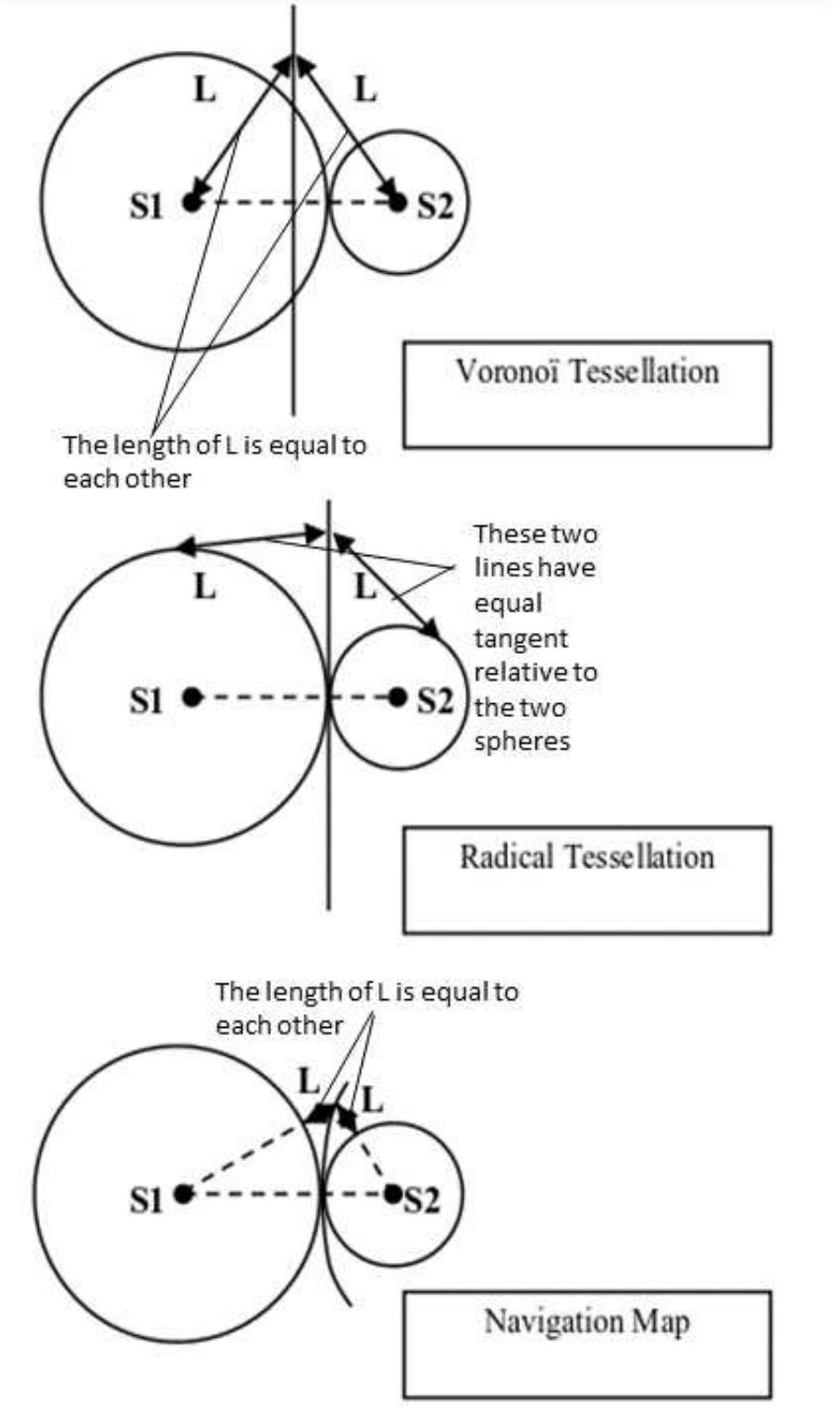

Figure 7: Different tessellation for packing of sphere of different size from Riccardo (2008)

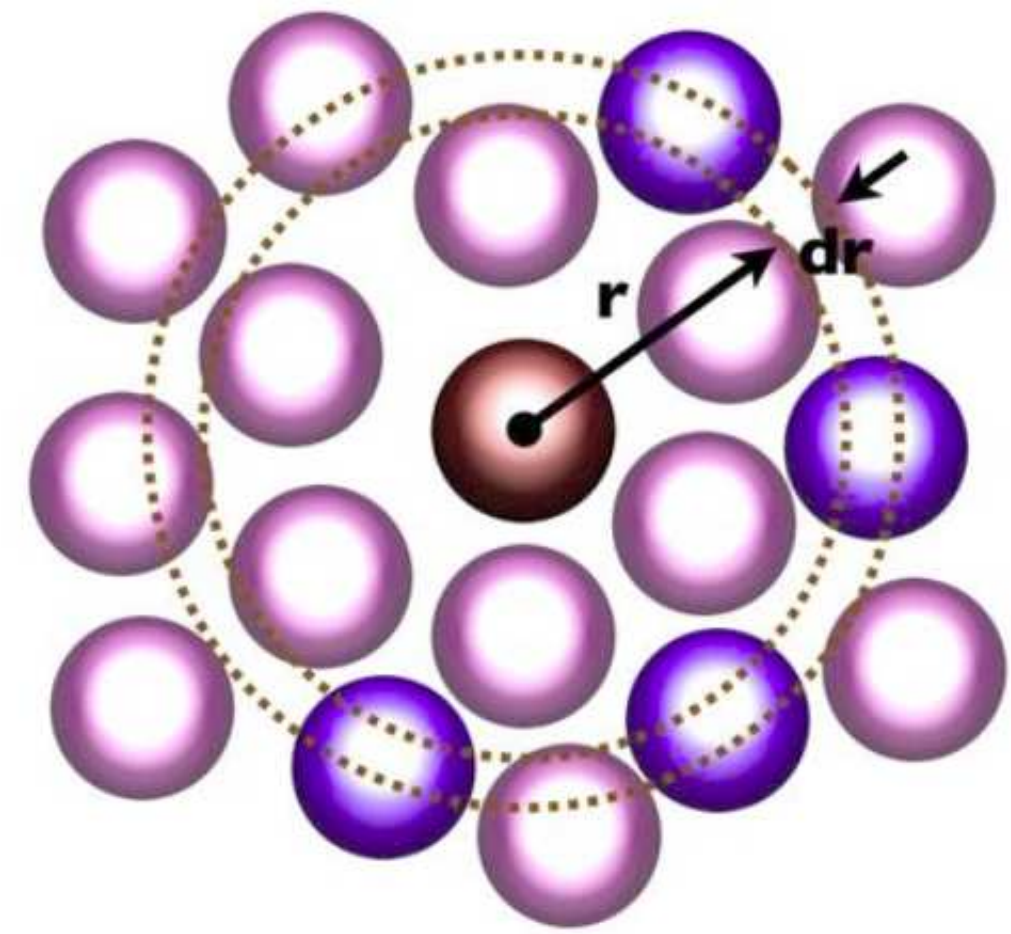

Figure 8: Radial Distribution Function

3.1.4 Coordination number

The definition of the coordination number is the number of contacts that a particle has with other particles. The simplest formula used to calculate this parameter is given by,

$$Z = 2\frac{N_c}{N_p} \tag{20}$$

where N_c is the total number of contacts and N_p is the number of particles. The definition of contact in DEM is necessary because contacts that are used to calculate the coordination number should be fully engaged contacts that transmit inter-particle force. The potential

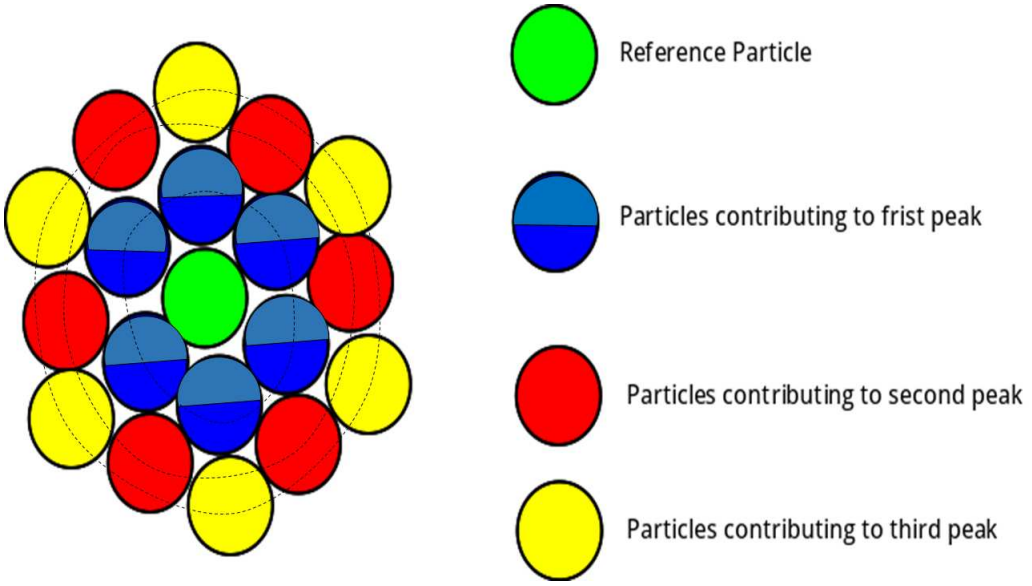

Figure 9: 2D example of particles contributing to the various peaks of the RDF

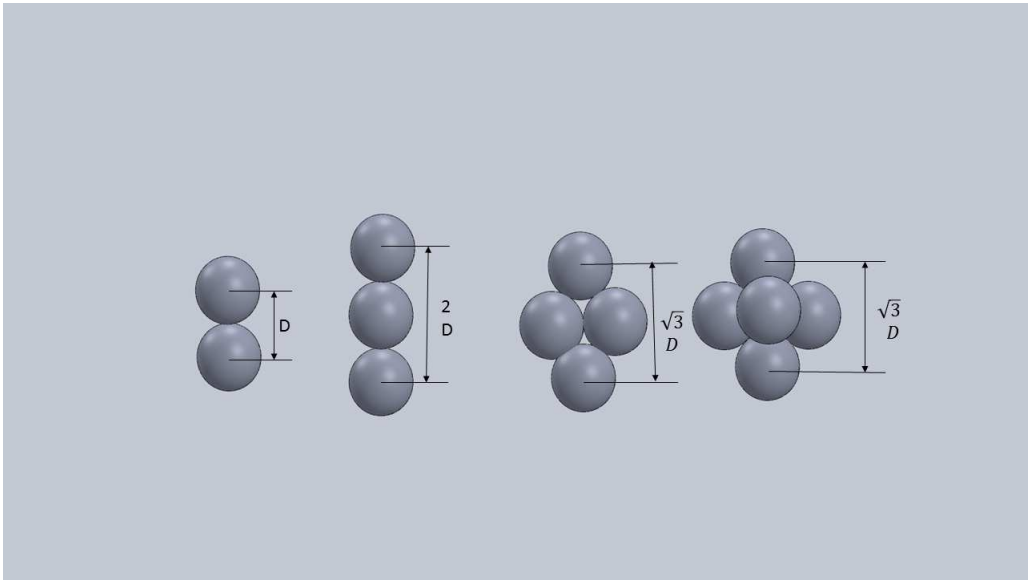

Figure 10: Sphere structures contributing to the main peaks of the RDF

contacts which do not transmit inter-particle force should be eliminated.

3.1.5 Coordination number for coarse particles

Binary mixtures of coarse particles were simulated in this study. Coarse particle packings are simpler than fine particle packings since the influence of cohesive forces and friction in

packings of coarse particle are negligible due to the fact that coarse particle packing is gravity-dominated problem. Before analyzing the results from any numerical model, it is important to have a basic understanding of the coordination number of mono-sized particle packings since the method used to study bi-disperse sphere packings is derived from this special case.

The coordination number is the most straightforward parameter in characterizing particle packings and assists in understanding the local configuration within the packing. The stability of each particle can also be obtained from the study of the coordination number (Aste 2005) [20].

Many theories about the coordination number for mono-sized packings have been developed from both numerical and experimental perspectives. Aste (2005) [20] noted that Newton's equations for the balance of the force and moment acting on each particle must be satisfied when all particles are settled in mechanical equilibrium. The number of constraints at each particle should be equal to the total number of degrees of freedom for each particle to achieve stability of the packing. The number of degrees of freedom should also be considered in terms of theoretical and practical aspects. For the theoretical case, the packing of N frictionless spheres has 3N degree of freedom (this refers to translational modes only, without consideration for any rotations), while the constraint for a single particle is equal to CN/2 (one contact for a single frictionless sphere provides a single normal force, where this one force constrains motion of the particle in that direction. For translational modes, two contacts at one particle are able to constrain one degree of freedom since the positive and negative directions along the axis between two contact points are constrained by two normal forces caused by the contacts. C is average contact, which is equal to summation of the number of contacts in the system divided by the total number of particles , and each contact shared by two spheres). Hence C must be 6 to achieve stability. For the practical case, the packing of N frictional spherical particles usually has 6N degrees of freedom (3 translation modes and 3 rotational modes) since friction always exists at particle contacts.

Constraint for a single particle is equal to 3CN/2, so C must be 4 for this case. However, this condition for C is neither sufficient nor necessary. Indeed, there can be local configurations that contribute to C but do not contribute to the whole system rigidity. To the authors understanding, this condition is only true when the wall effect of the packing of particle is eliminated from consideration

Silbert (2002) [18] confirmed this interpretation in numerical simulations. He claimed that this theory is true when packings of frictionless hard spheres are simulated. But packings of frictional hard spheres show disagreement with the theory, where the average coordination number decreases from 6 to 4, causing some doubt on this general claim.

3.1.6 Coordination number: experiments versus models

In practice, there are usually errors between experimental and numerical results. Theoretically, the discrete element method has been proven to be an effective tool to study packings of granular material when compared with a wide array of experimental results. In numerical simulations, the condition of contact is simple: for two spheres with radii r_1 and r_2, the condition that two spheres are in contact is achieved when

$$d = r_1 + r_2 \tag{21}$$

where d is the distance between the center of two particles. But in experiments, it is difficult if not impossible to measure positions of each particles in a system accurately due to the unavoidable technical approximations such as threshold distance. Some experiments that have been conducted to empirically estimate the coordination number are mentioned below.

Early stages of estimating the coordination number were compared with physical experiments. Smith et al. (1929) [19] poured lead shots into beaker, and then filled the beaker with a solution of acetic acid. Some white regions appeared at the contact points of lead shot due to capillary necks of acid. The number of white dots on each individual lead shot

was counted as a contact (coordination number). However, results of this early experiment were not completely accurate since it is impossible to distinguish touching spheres and near but non-touching spheres. Bernal and Mason (1960) [19] conducted a similar experiment by ball bearing compressed with a rubber band. The contacts of touching ball and nearly touching ball were counted separately. A different method used by Scott (1962) involved pouring molten paraffin wax into a heated container filled with balls, and the contacts of balls were counted. In recent years, confocal microscopy and x-ray microtomography have been used to visualize the packing structure of particles. Aste et al (2004c; 2005d) [19] conducted empirical investigation of large packing of mono-sized spheres by X-ray computer tomography, leading to overall comportment of predicting this quantity.

3.1.7 Relationship between coordination number and void ratio

According to experiment observations, the coordination number decreases as the void ratio increases. To determine the relationship between the coordination number and void ratio, many empirical formulas has been developed based on data from experiment. Field (1963) [21] proposed the formula,

$$Z = \frac{12}{1+e} \tag{22}$$

$$e = \frac{V_V}{V_S} \tag{23}$$

where Z is the coordination number, e is void ratio, V_V is the volume of void-space and V_S is the volume of solids. Mitchell (1993) [21] suggested that for packings of mono-size rigid spheres,

$$Z = 26.386 - \frac{10.726}{e} \tag{24}$$

Aste (2004c; 2005d) [21] experimentally studied the relationship of large packings of mono-sized spheres. They assumed that the spheres in contact are located at a radial distance between the diameter d and d + v, where v is the voxel-sizes i.e. the size of the pixels used during the image acquisition. The plot of the relationship between packing density and coordination number is shown in Figure 11.

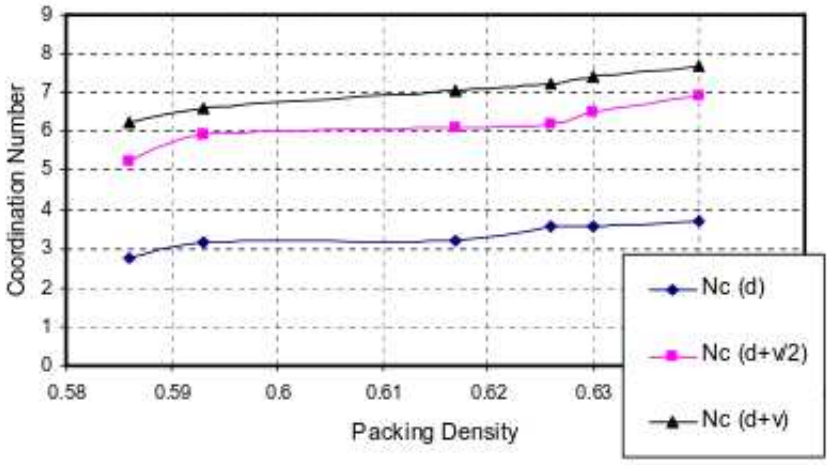

Figure 11: Coordination number as a function of particle density

Rothenburg and Kruyt (2004) found the relationship between coordination number and void ratio to be highly dependent on anisotropy of the contact orientation. Hasan and Alshbli (2010) [21] demonstrated that there is a difference between empirical formulas developed from sand and formulas from an ideal material such as glass balls. The relationship between coordination number and void ratio varies with particle shape, surface roughness, and particle-size distribution. Empirical formulas appear to be valid only for very specific conditions.

The results of Yang et al. (2003b) [21] confirm that there is a one-to-one relationship between porosity and microstructural properties such as coordination number so that the

microstructural information of a packing can be mapped by the porosity of the packing. This is consistent with the finding of Jullien et al. (1996) [21] for coarse particles. Therefore the quasi-universality may exist for the packing of particles with porosity as high as 0.8. This finding provides a good explanation why, in engineering practice, porosity or its related parameter such as packing density can alone characterize a packing of granular particles.

3.1.8 Partial Coordination Number

Pinson et al. (1998) noted that previous experimental studies do not provide complete information about coordination number. For example, a binary mixture gives three types of contacts (which are known as partial coordination numbers): large-to-large, large-to-small or small-to-large and small-to-small, and each type of contact should have its own distribution. In engineering practice, this parameter can be extremely useful. For example, the shear behavior of material from co-disposal primarily depends on large-to-large particle contact since large-to-large particle contact change with mixture ratio as shown in Figures 12 and 13,

3.2 DEM solutions

The work that follows is based on the DEM solver LIGGGHTS [22]. This is an improved version of LAMMPS, a parallel particle simulator at the atomic, meso, or continuum scale. LAMMPS offers implementations for both linear (Hooke) and non-linear (Hertz) granular potentials. LIGGGHTS improves these features for granular simulations, comprising geometries imported from CAD files and a moving mesh capability, features for particle insertion and packing, multiple contact models, non-spherical particle handling by means of the multi-sphere method, a bonded particle model, wall-stress analysis and wear prediction, and a 6 degree-of-freedom capability for rigid bodies.

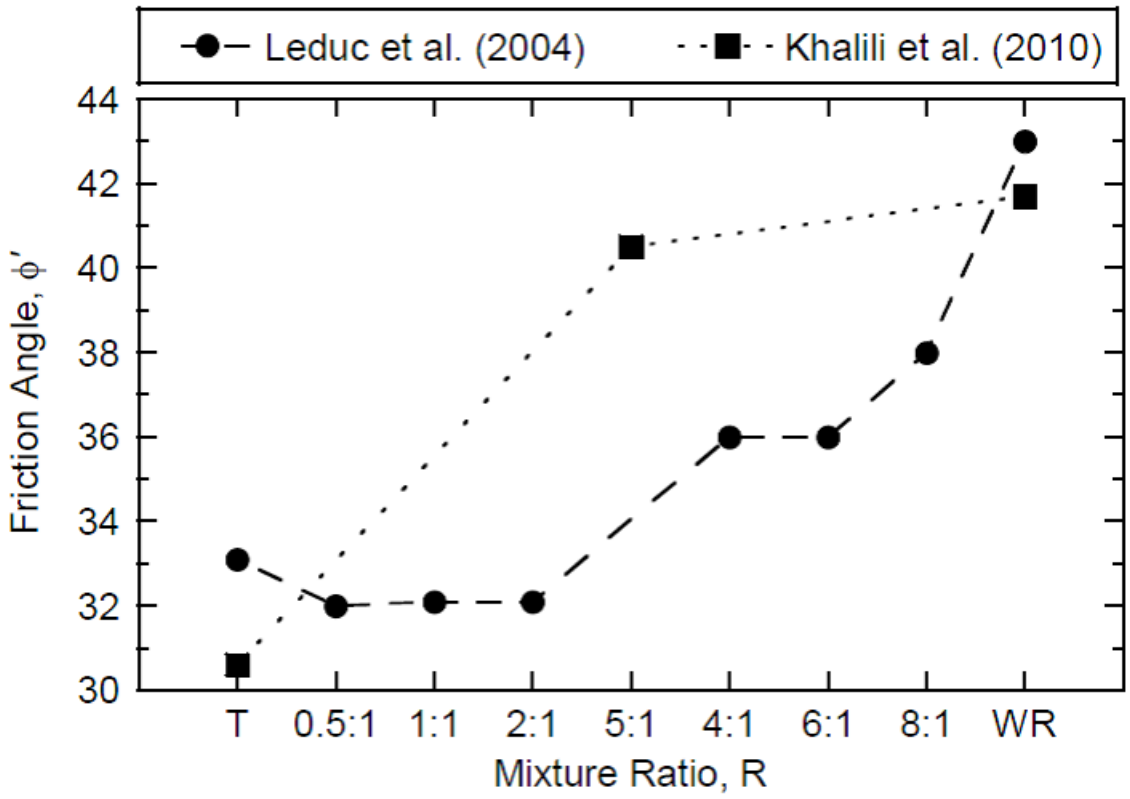

Figure 12: Relationship between effective stress friction angle and mixture ratio of waste rock (WR) to tailings (T), based on dry mass. Data obtained from Leduc et al. (2004) and Khalili et al. (2010).

3.2.1 Comparison: Packing of uniform spheres

To validate result from LIGGGHTS, a comparison was first made with the work of Zhang (2001) [1]. Results have been compared in term of packing density, coordination number and the radial distribution function. In Zhang (2001) [1], uniform spheres of a constant diameter (d = 10 mm) were poured at varying dropping heights, where the condition of a dropping height of 20 sphere diameters was selected to be simulated in the present work. The deposition intensity was set to 3000 particles per second where the particle enters the control volume at the top of the cylindrical domain. A schematic of the model is shown in Figure 14.

Zhang (2001) [1] used 5000 mono-size particles that were poured into a cylindrical container whose diameter is 24 sphere diameters. Spheres were inserted from an upper opening

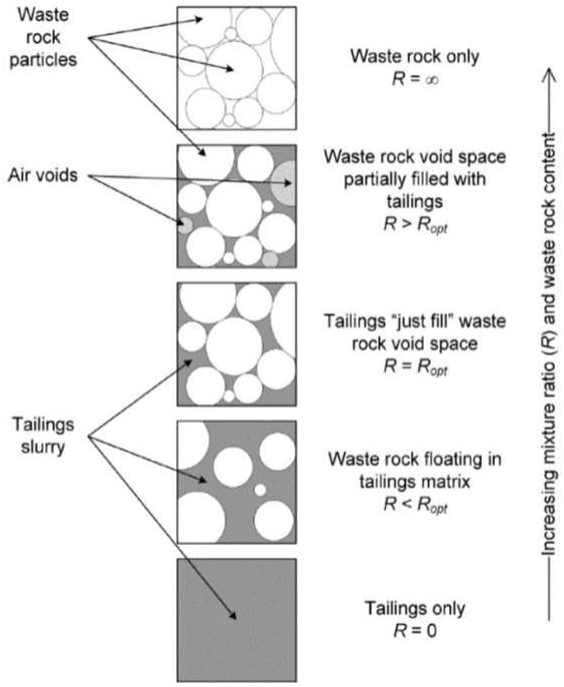

Figure 13: Particle structure of co-mixed waste rock and tailings for different mixture ratios from Wickland (2006) [3]

whose diameter was 0.8 times the container diameter. The particles were inserted via batch-wise dropping, which means that particles were inserted at a rate of approximately 750 particles every 1 s (i.e., 10000000 time steps for Δ t= 0.0000001 s) as shown in Figure 15. A small velocity (-0.05 m/s), in addition to gravity, was assigned to each particle in the system. This velocity of particles in the present model is different from Zhang's model, which assigned a small velocity with random direction. The material properties of the particles were as follows: restitution coefficient is 0.3, friction coefficient of particles is 1.13, Particle density is 2500 kg/m^3, Young's modulus is 60 GPa, Poisson ratio is 0.25.

In the present model, the coefficient of restitution was set to be 0.3 to calculate velocity loss during impact since the damping coefficient is not an input coefficient in LIGGGHTS. As noted by Zhang (2001) [1], there is a relationship between the damping coefficient and the coefficient of restitution for specific materials. The resulting relationships are shown in Figure 16. Zhang (2001) [1] used a damping coefficient to 0.3 in their DEM model.

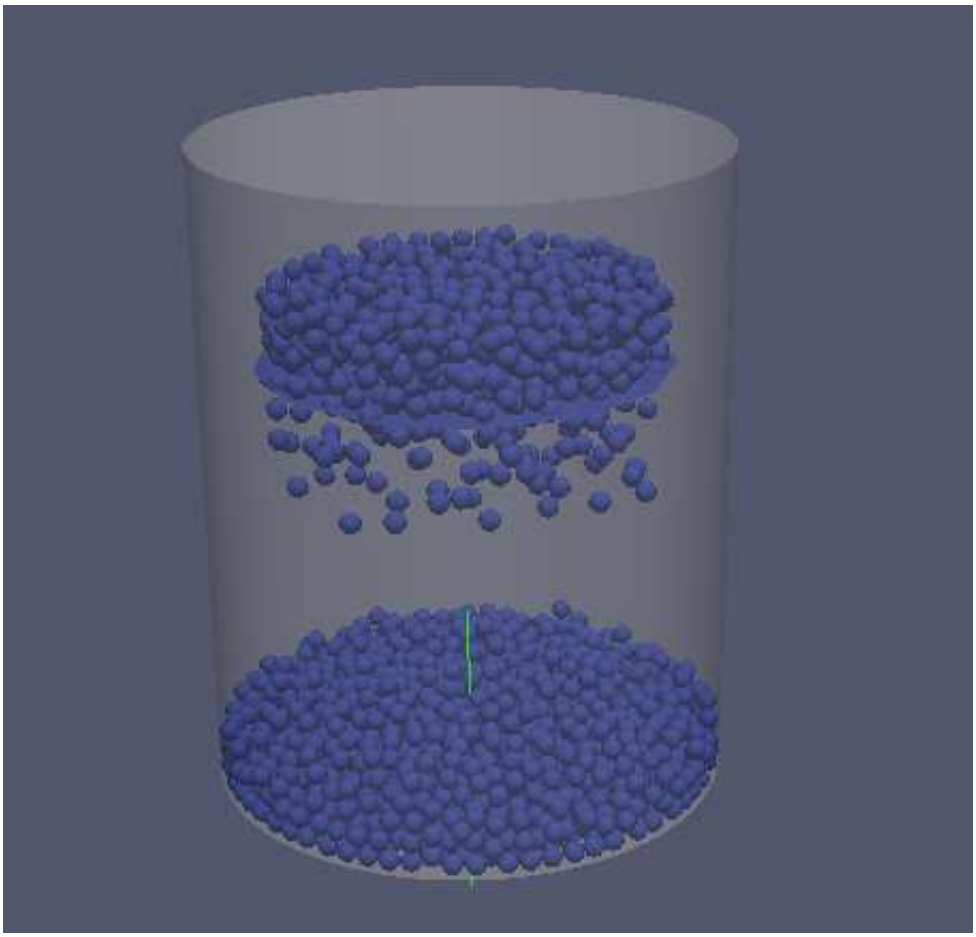

Figure 14: Illustration of the filling and packing process in our simulation

According to Figure 16, the coefficient of restitution is equivalent to damping coefficient when the damping coefficient is equal to 0.3.

The packing density was calculated using the area within a section three sphere diameters away from the bottom and top surfaces. The mean coordination number was equal to the summation of the coordination number of each particle in the system divided by total number of particles in the system. In the formula used to obtain the radical distribution function, Δr was set to 0.02. The comparison between DEM results from the simulation conducted in this study and Zhang (2001) [1] is shown in Table 1

The RDFs from Zhang (2001) [1] and the present model are shown in Figure 17a and 17b.

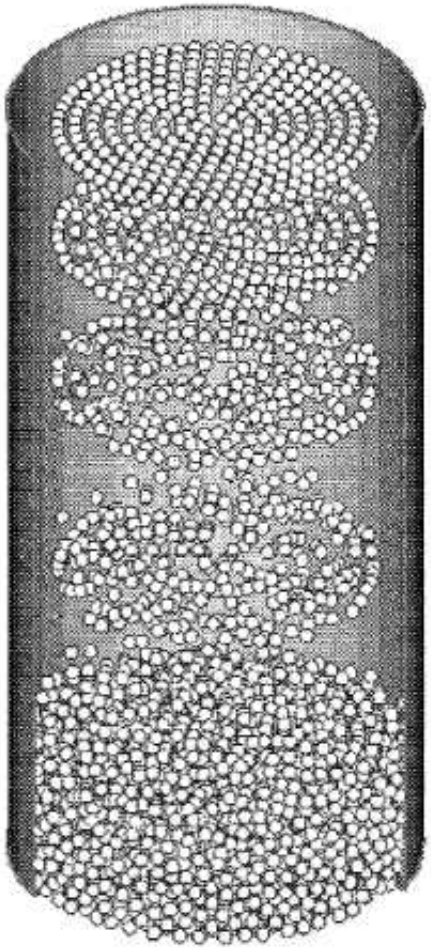

Figure 15: Illustration of the filling and packing process in Zhang (2001)

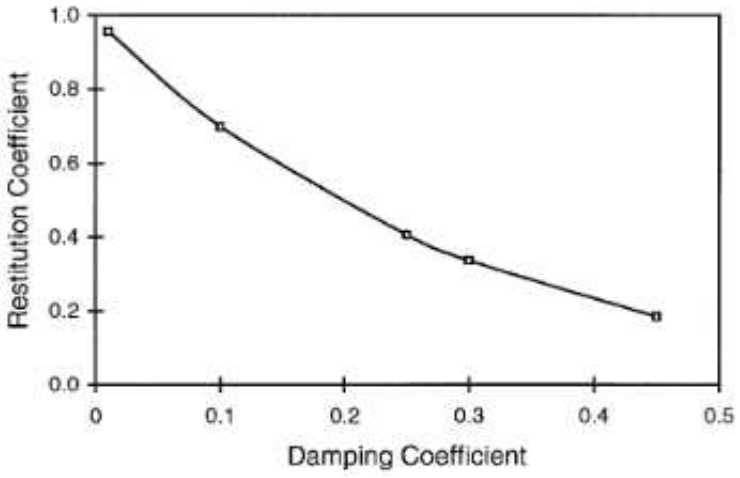

Figure 16: Restitution coefficient as a function of damping coefficient (Zhang 2001) [1]

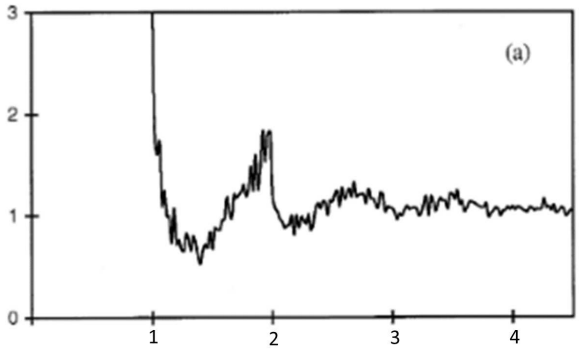

(a) Radial distribution function from Zhang (2001) [1]. The X axis is radial distance from center (sphere diameter=0.01), Y axis is average number of sphere center

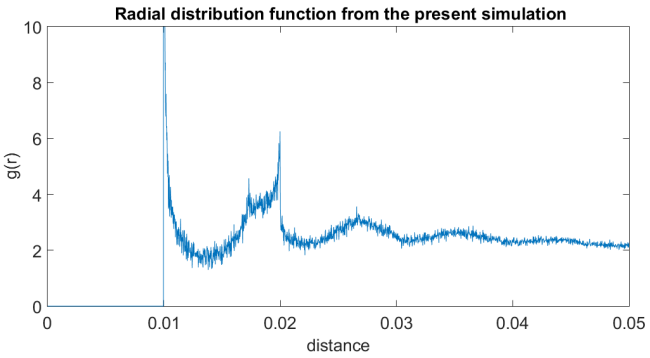

(b) Radial distribution function from the present model,X axis is Radial distance from center (mm), Y axis is avenge number of sphere center

Figure 17: Comparison of radial distribution function (RDF) from Zhang (2001) [1] and the present model

Table 1: Comparison of result

	Packing density	Mean coordination number
Zhang (2001)	0.551	5.55
Present	0.583	4.655

The radial distribution functions are in good agreement. As expected, both have two splittings in the second peak. The first component is less sharp than the second. The value of the packing density from the present simulation is six percent larger than that of Zhang (2001) [1] and the mean coordination number is twenty percent smaller. The differences may be caused by slightly different packing methods of the two models. Specifically, the orientation and magnitude of initial velocity of particle is not exactly the same. Additionally, the difference of the mean coordination number may caused by the different critical distances. In the present work, the critical distance is set to 1 d since the critical distance in LIGGGHTS can not be changed. Zhang (2001) [1] used 1.01 d. The overall agreement between the two models is reasonably good.

3.3 Description of model: Bi-disperse mixing

Packing methods of binary mixtures can include three other variables according to evidence from previous literature (Zhang 2001) [1]. The geometry of the disruptor which is meant to the slanted lines and semi-circle barriers in the present models was studied as the primary variable in this thesis. Six different geometries have been used in the numerical simulations to determine their influence on packing structure of binary mixtures. The complexity of geometry of these disruptor is quantified by the length and position of the disruptor elements: Model A (0), Model B (50), Model C (47.1), Model D (97.1) Model E (97.1), Model F (147.1). In this work, the regularity of the packing structure is quantified by three measures: the packing density, coordination number and radial distribution function. The total number of particles varies as discussed below.

3.3.1 Packing method

In the simulations that follow, two types of particles are inserted from two quadrilateral openings at the top of the modeled domain. The initial determined velocities are set to 1 m/s in vertical direction. The deposition intensity of the larger particle is 350 particle/s. Deposition intensity of smaller particle is 1050 particle/s.

3.3.2 Particle properties

The material properties of the larger particles have a diameter (d) = 0.02 m. The material properties are E =700 GPa, $\nu = 0.3$, Coefficient of Restitution, Coefficient of Rolling friction and Friction coefficient is 0.15,0 and 0.2 for smaller particles to larger particles, larger particles to larger particles, larger particles to wall. The smaller particles have a constant diameter of d = 0.005m with E = 700 GPa, ν = 0.3, Coefficient of Restitution, Coefficient of Rolling friction and Friction coefficient is 0.15,0 and 0.2 for smaller particles to larger particles, smaller particles to smaller particles, smaller particles to wall. The material properties of the wall were E = 7000 GPa, ν = 0.3. The particle density for both particle sizes was 2700 Kg/m^3.

3.3.3 Geometry of the Numerical Experiments

The purpose of designing these six disruptor is to determine the effect of disruptor elements (slanted lines and semi-circle barriers). As shown in Figure 18 from Model F, The slanted lines force particles move toward to the center line of disruptor, and the semi-circle barriers force particles move toward to two side wall of disruptor. The geometer of disruptor is shown in Figure 19- Figure 25,

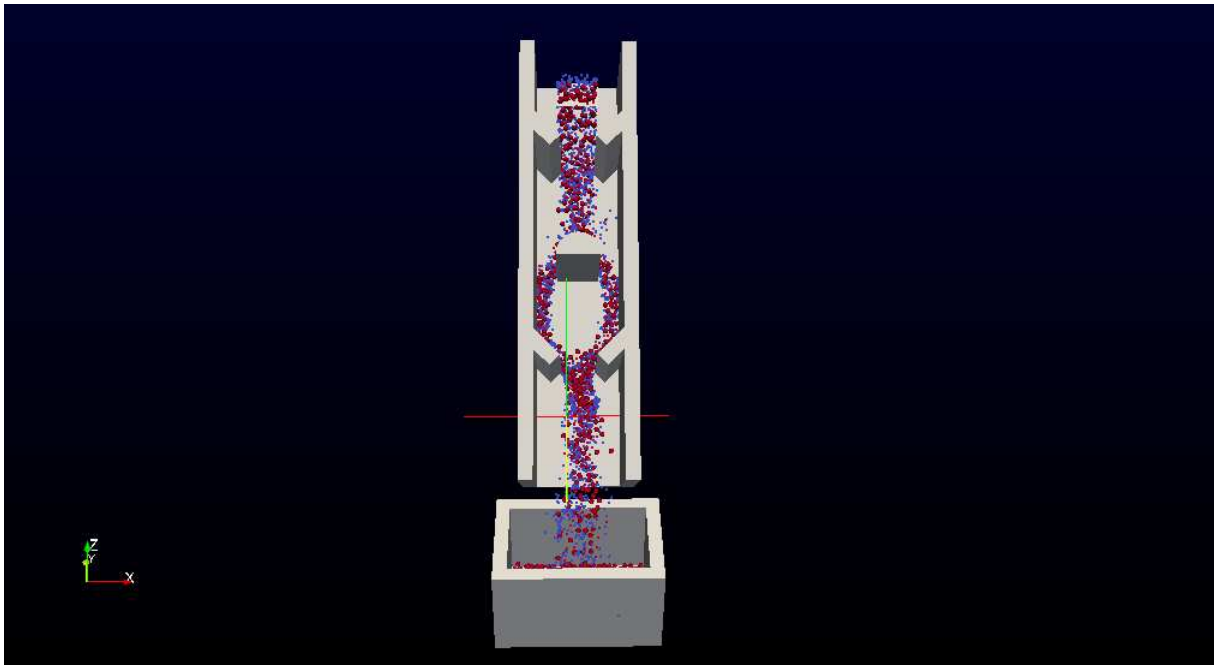

Figure 18: Screen shot from Model F

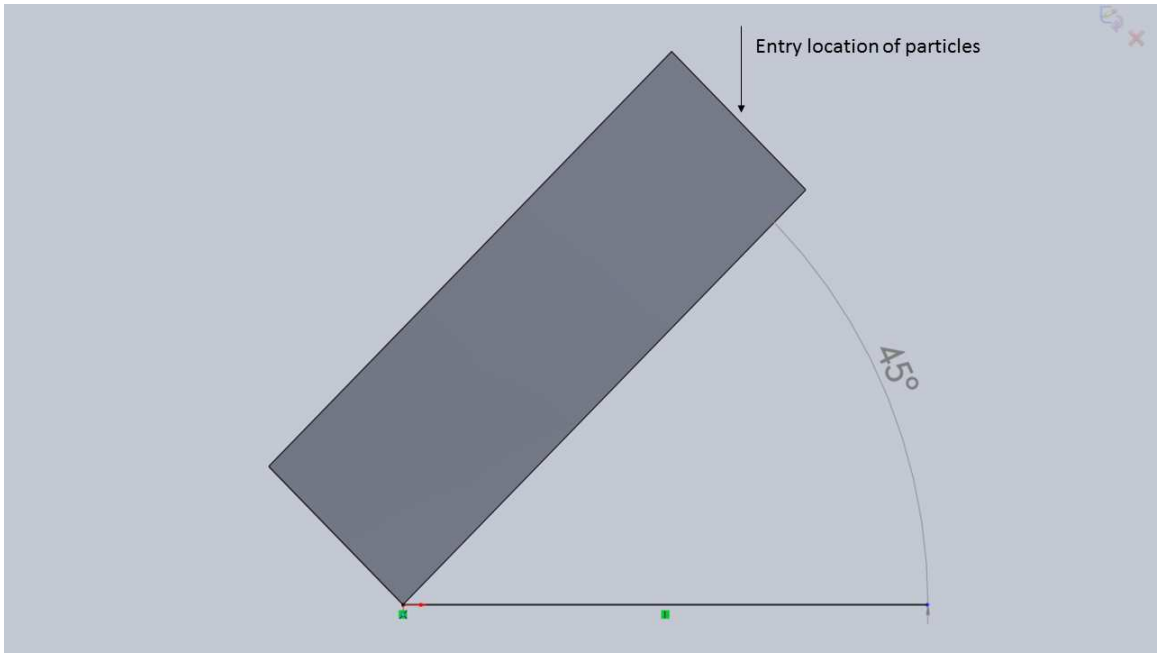

Figure 19: Side view of all disruptors

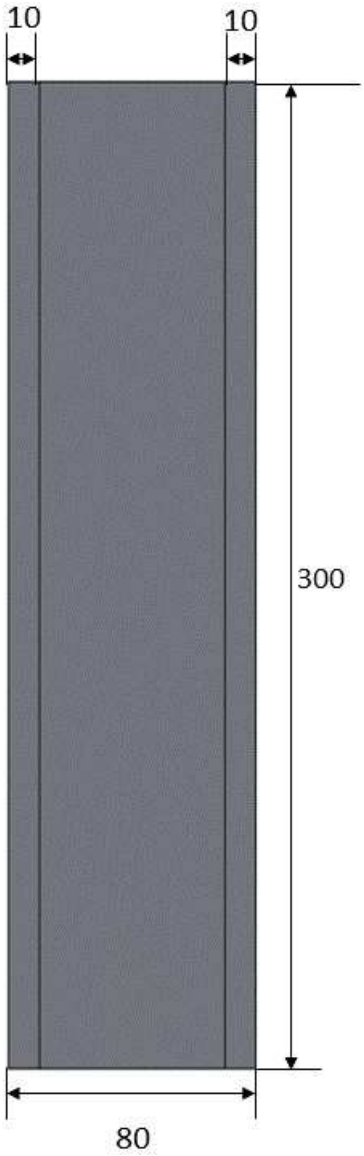

Figure 20: Geometry of Model A (all dimensions in mm)

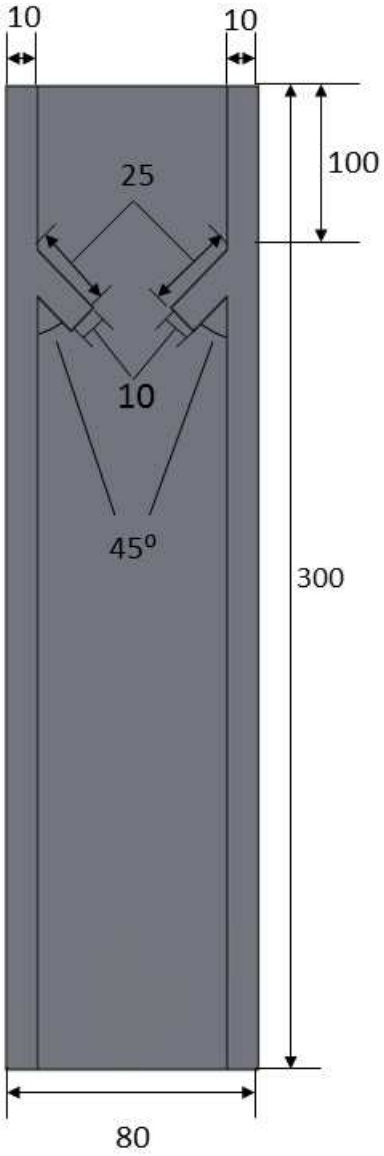

Figure 21: Geometry of Model B

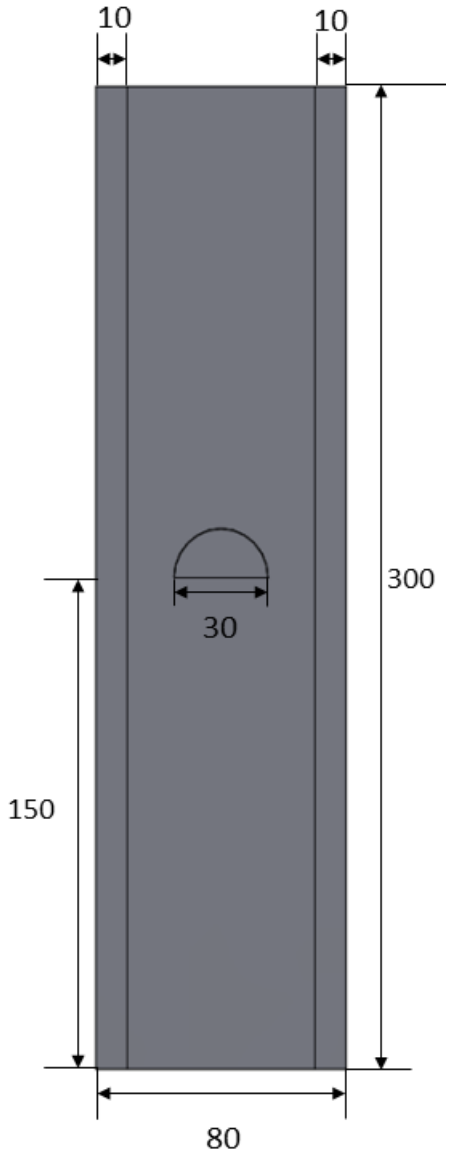

Figure 22: Geometry of Model C

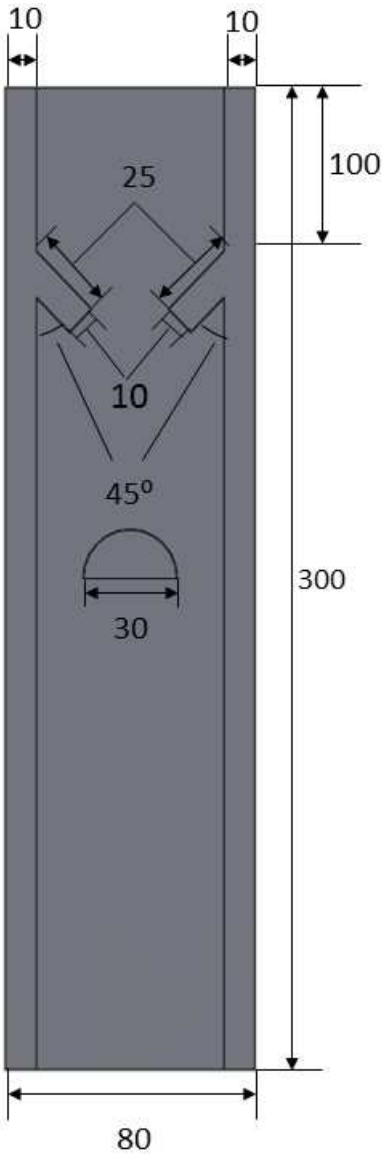

Figure 23: Geometry of Model D

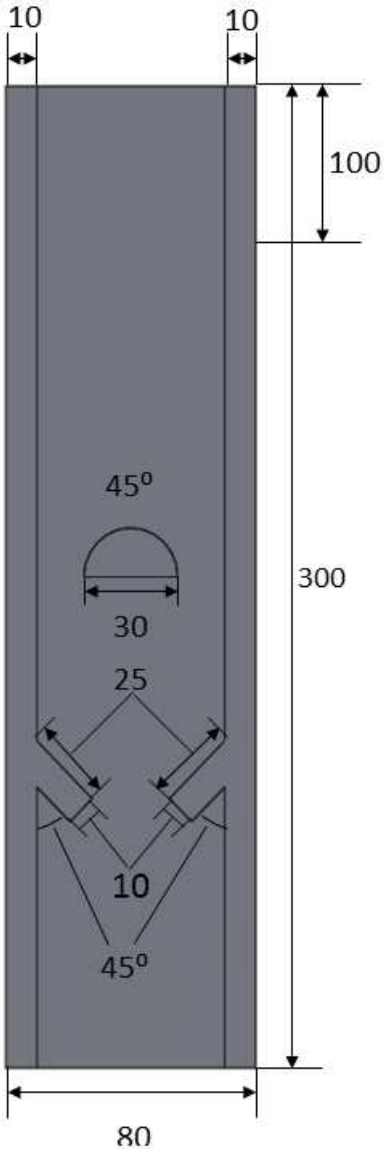

Figure 24: Geometry of Model E

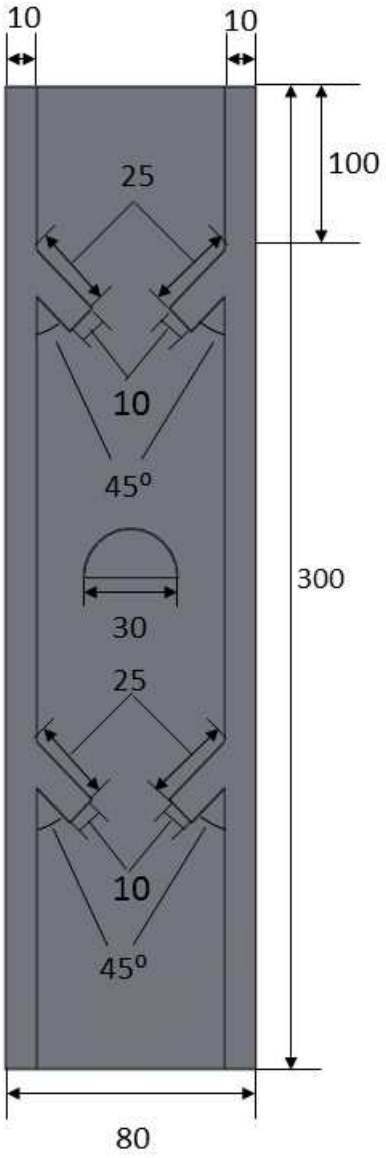

Figure 25: Geometry of Model F

3.3.4 Hertz history contact model in LIGGGHTS

It is useful to review the nature of the specific contact model as it is used in the numerical simulations that follow. In conventional DEM methods, there are three common and well-established contact models:

1. a linear model based on a Hooke-type relation;

2. a non-linear model based on the Hertz theory for the normal direction and the no-slip solution of the theory developed by Mindlin and Deresiewicz (1953) [13] for the tangential direction; and

3. a non-linear model with hysteresis based on the complete theory of Hertz and Mindlin and Deresiewicz (Mindlin and Deresiewicz 1953) [13] for elastic frictional collisions.

There are two contact models in LIGGGHTS. The first is a nonlinear type model based on Hertz theory. The second is a linear model, based on a Hooke-type relation. Contact force calculations are the most time consuming task in DEM simulations. Contact models should be chosen carefully since there is a trade-off between accuracy and efficiency. It is extremely important to determine if accuracy can have significant improvement when complex contact models are used. Alberto (2004) [23] made a comparison between these three contact models and compared the result from numerical models to experimental result, and found that linear models are sufficient for most cases. For the case that needs more details from macroscopic scale, such as normal and tangential forces, velocities and displacements, the Hertz and Mindlin and Deresiewicz model is more appropriate. The most complex model based on the complete theory of Hertz and Mindlin and Deresiewicz for elastic frictional collisions show worse agreement with experiment under some conditions such as low values of the impact angle.

To obtain more accurate results, the nonlinear type model based on Hertz theory in LIGGGHTS is used in this study since details pertaining to normal and tangential force were of primary not interest. The nonlinear model based on Hertz theory in LIGGGHTS is slightly different from the Hertz model listed in number 2 above. The quantities used to

calculate the normal and tangential forces are in the following equation,

$$F_n = (K_n \delta_n - \gamma_n v \cdot n_{ij}) n_{ij} \tag{25}$$

$$K_n = \frac{4}{3} Y^* \sqrt{R^* \delta_n} \tag{26}$$

$$\gamma_n = -2\sqrt{\frac{5}{6}} \beta \sqrt{S_n m^*} \tag{27}$$

$$\beta = \frac{\ln(e)}{\sqrt{\ln^2(e) + \Pi^2}} \tag{28}$$

$$S_n = 2Y^* \sqrt{R^* \delta_n} \tag{29}$$

$$m^* = \frac{m}{2} \tag{30}$$

where F_n is normal force, K_n is normal stiffness, n_{ij} is the unit vector point from i th particle to j th particle, e is the coefficient of restitution of the particles, R^* is the effective radius that is the geometric mean diameter of the i th and j th particle, Y^* is particular Youngs modulus which is calculated in terms of Youngs modulus, δ_n is the overlap in normal direction, γ_n is

viscoelastic damping constant for normal contact respectively. Additionally, these relations also hold:

$$F_t = (K_t|\xi_t| - \gamma_t v \cdot t_{ij})\frac{\xi_t}{|\xi_t|} \tag{31}$$

$$K_t = 8G^*\sqrt{R^*\delta_n} \tag{32}$$

$$\gamma_t = -2\sqrt{\frac{5}{6}}\beta\sqrt{S_t m^*} \tag{33}$$

$$G^* = \frac{Y}{4(2+\sigma)(1-\sigma)} \tag{34}$$

$$S_t = 8G^*\sqrt{R^*\delta_n} \tag{35}$$

where F_t is the tangential force, K_t is the tangential stiffness, m^*=$m/2$ and ξ_t is the tangential displacement vector between two spherical particles which is truncated to satisfy a frictional yield criterion, t_{ij} is unit vector that is perpendicular to normal direction and is opposite to the direction of deformation and independent to the direction of velocity, and γ_t is viscoelastic damping constant for tangential contact.

3.4 Evaluation of variables

Since numerous variables have been proposed in the literature that can be used to classify packings, it is necessary to limit this study to those that have a significant effect on the packing structure of binary sphere mixtures. An evaluation of the importance of different variables has been conducted below.

Marcrae (1960) [24] found that packings of mono-sized particles could be affected by particle properties, container properties and packing method (mode of deposition). Zhang (2001) [1] confirmed this finding using DEM simulations with the mixing of two assemblies of particles with different diameters were mixed. This type of mixture is called a binary mixture and is a common study topic in geomechanics. Wickland (2006) [3] found that packings of binary mixtures for two specific materials can be influenced by the particle size ratio, the mixture ratio, and the density of packing for each particle type.

According to the evidence found in the literature, possible significant variables in binary sphere mixture are listed below.

1. Material properties: a. Young's modulus ratio; b. Restitution coefficient ratio; c. Ratio of Poisson ratio; d. Friction coefficient ratio; e. Sliding friction coefficients; f. Rolling friction coefficients; g. The Hamaker constant; h. Particle density.
2. Ratio of diameters of two types of spherical particles.
3. Density of packing of each type of particle.
4. Mixture ratio
5. Packing method
6. Container: wall effect

Below the variables used in the present study are described.

3.4.1 Material properties

Two types of coarse particles were used in the simulations to mix particles via geometric disruptor. In this case, dynamic variables in the material properties should not be ignored. The coefficient of restitution ratio and friction coefficient ratio were both considered. Zhang (2001) [1] found that the packing structure for coarse spherical particles is strongly influenced by the restitution and friction coefficients and confirmed this by numerical and experimental study. As shown in Figures 26-28, Zhang found that packing density and coordination number increase with restitution coefficient and decrease with friction coefficient.

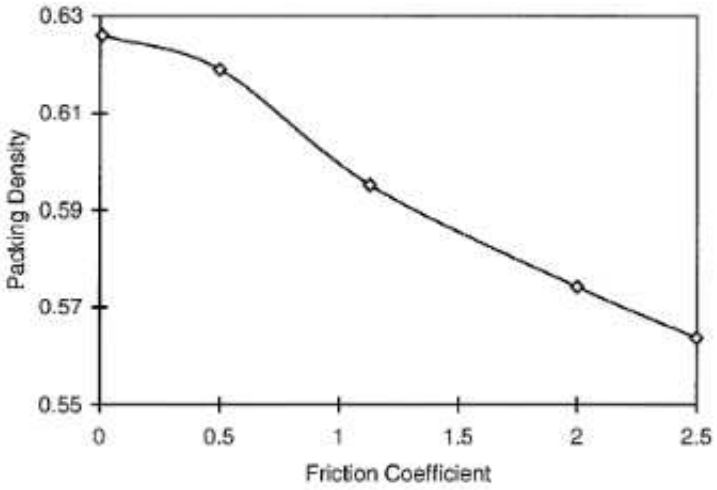

Figure 26: Effect of friction coefficient on packing density obtained when dropping heights= 49d, damping coefficients= 0.3, and deposition intensity= 1000 particles/s. (Zhang, 2001)

In civil engineering fields such as mining, studies are mainly focused on mixing of coarse particles. So the packing behavior of coarse particles is different from that of fine particles. Packing behavior of coarse particles tend to depend on space filling properties of particle, since the packing of coarse particles is a gravity-dominated problem (Latham, 2000) [25]. Fine particles are those with diameters less than 100 um. Yang (2003) [26] found that particle properties (the sliding friction coefficients, rolling friction coefficients, the Hamaker constant and particle density) have influence on packing behavior of fine particle since inter-particle forces dominate (such as van der Waals force and electrostatic force) over gravity force, so

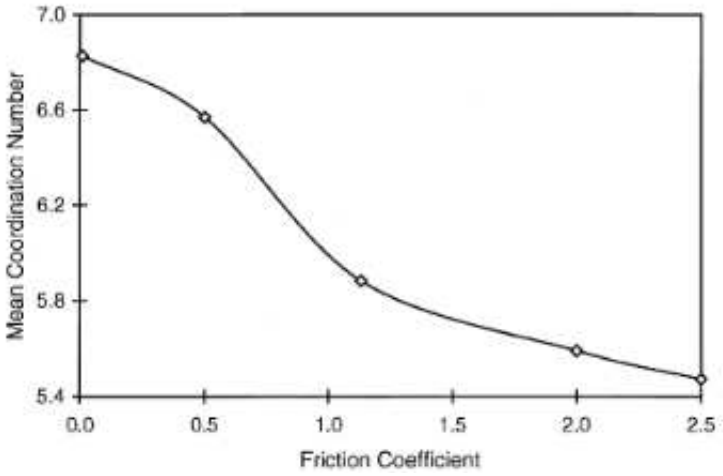

Figure 27: Variation of mean coordination number with friction coefficient, corresponding to the conditions in Fig.26 (Zhang, 2001) [1]

some material proprieties related to the inter-particles force are not important variables in the binary mixture of coarse particles.

3.4.2 Particle size ratio

The particle size ratio affects the space filling properties of the particles. In a binary sphere mixture, the particle size ratio is equal to the ratio of diameters of the two types of particles. Marcare (1960) [24] found that the presence of larger particles reduces the porosity of the bulk packing and the particles that are small enough to fill the voids between larger particles also reduces the porosity of the bulk packing. Smaller particles must be smaller than a "critical ratio of entrance" to fill the voids between the larger particles. As shown in Figure 29, the critical ratio of entrance for the tightest ordered packing should be less than a 7:1 sphere particle size ratio as found from experiment (Graton and Fraser 1935) [27].

3.4.3 Mixture ratio

In binary mixtures, the mixture ratio can also have a significant effect on the structure of the final packing. The definition of the mixture ratio is the ratio of large to small particles in

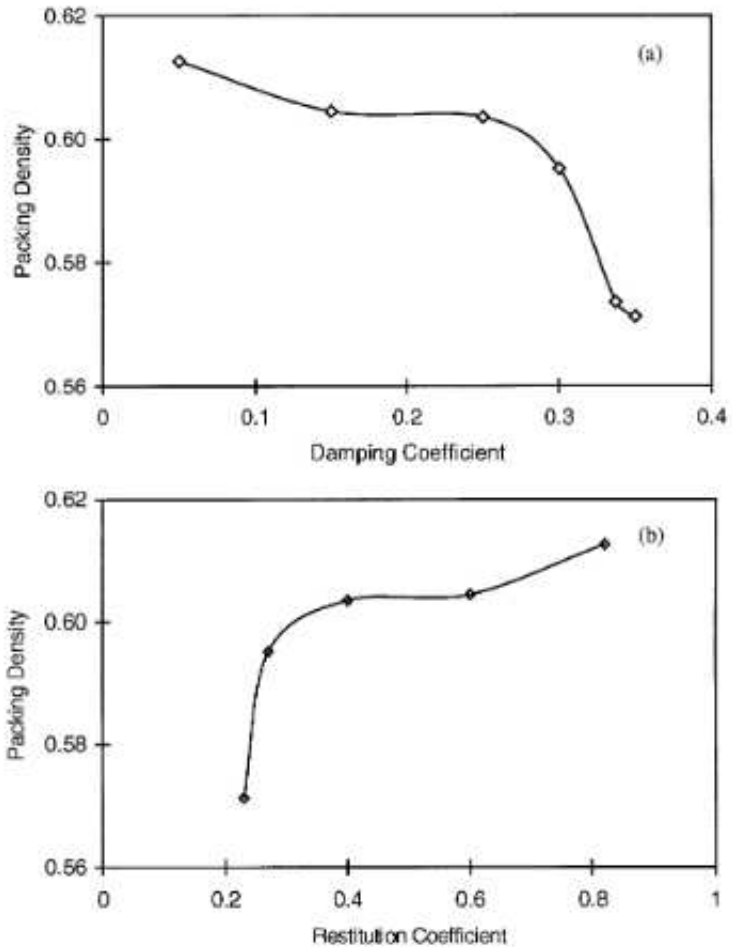

Figure 28: Dependence of packing density on damping coefficient (a) or restitution coefficient (b) obtained when dropping heights = 49d, friction coefficients=1.13, and deposition intensity = 1000 particles per second (Zhang, 2001) [1]

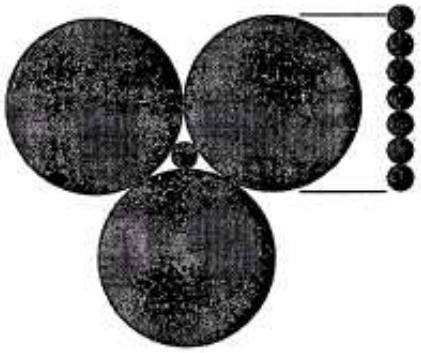

Figure 29: Critical ratio of entrance for round shapes(Graton and Fraser 1935)

term of overall volume or mass. Fraser (1935) [27] showed that smaller particles just fill voids between larger particles when volumetric-based mixture ratio is equal to 0.7. The optimum mixture ratio (0.7) is only true under the conditions used in Fraser's experiments, as shown in 30. The optimum mixture ratio in other cases will vary with other particles properties such as the size ratio and the density of packing of the individual particle sizes.

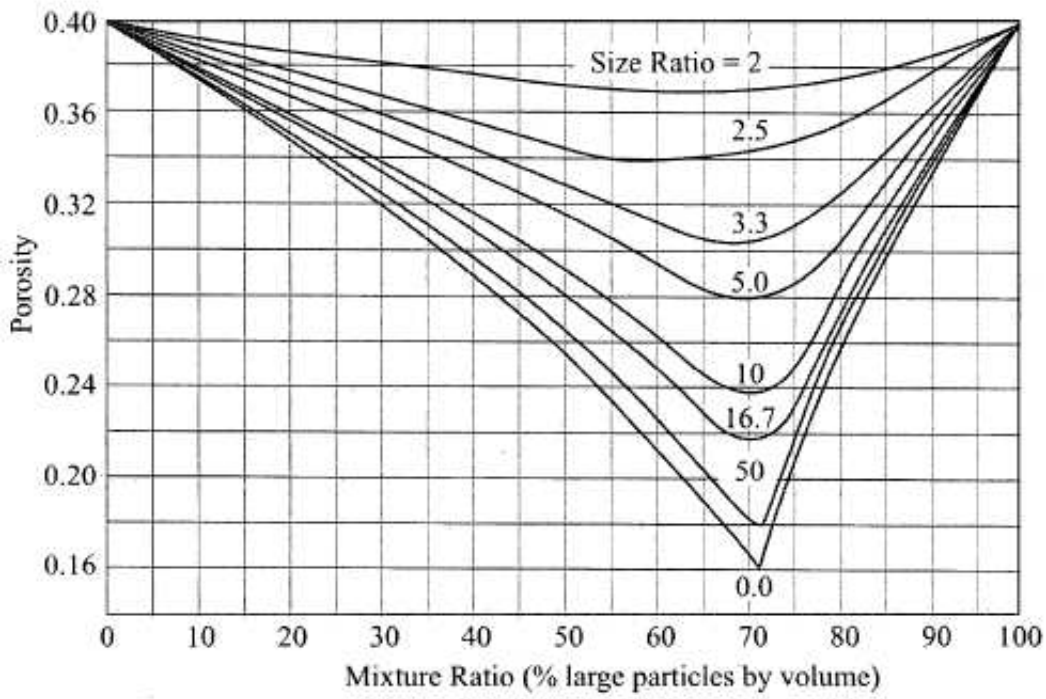

Figure 30: Experimentally determined porosity versus mixture ratio for binary mixture (Fraser 1935)

3.4.4 Packing method

Packing methods can strongly affect the packing of binary mixtures. Zhang (2001) [1] proposed that the dropping height and deposition intensity are two important variables in packing of particles. These two variables are related to the so-called bridge phenomenon that describe a stable arrangement of particles in which at least two of the particles depend on each other for their stability within the particle assembly. The relationship between the

dropping height and packing density is shown in Figure 31 The particle bridges are mainly a result of simultaneous settling motion of closely neighboring particles. The geometry of the disruptor also has an influence on packing behavior since it can alter the motion and settling of particles. It is this feature that is the primary focus of the present work.

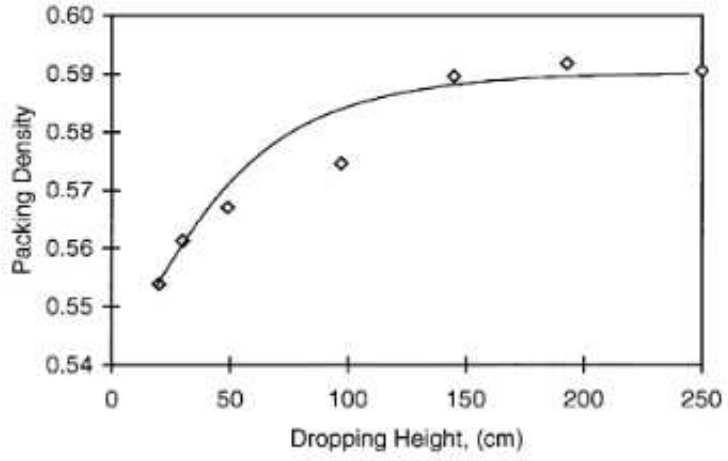

Figure 31: Effect of dropping height on packing density, obtained when deposition intensity = 3000 particles/s, friction coefficients = 1.13, and damping coefficients = 0.3 (Zhang, 2001). The dots are the results from experiment, and the line is the result from numerical analysis

3.4.5 Density of packing of each type of particles

The "just fill" point is extremely important in binary mixtures. In Figure 30, the lowest point of porosity for each size ratio is known as the just fill point. It means that smaller particles are just able to fill the voids of the larger particle skeleton. Figure 30 represents a case where the porosity of each type of particle mixture is 0.4. The result of position of the just fill point moves as the porosity of each type of particles changes. For instance, if larger particles have a smaller individual porosity, it will lead to the result that the just fill point moves to lower mixture ratio. To use the density of packing of each type of particle as a variable, it should be noted that this becomes a problem of packing for mono-sized particles for each type of sphere. It means that the particle size of each type of particle should be changed but the particle size ratio should stay the same value.

In conclusion, the important variables as used in this study are (1) restitution coefficient ratio, (2) friction coefficient ratio, (3) ratio of diameters of two types of particles, (4) mixture ratio, (5) packing method, and (6) density of packing of each type of particles. In the present study, the complexity of geometry of disruptor which is included in packing method is used as the variable, and the other variables are hold constant.

4 RESULT

In this chapter, the results of all simulations are presented. Each of the measurements reported below were computed using final particles positions of the settled particles after mixing was complete.

4.1 Coordination number

Calculation of the coordination number using the present model can be separated into five numbers: 1) mean coordination number of all particles, 2) mean coordination number of the smaller particles, 3) mean coordination number of the larger particles, 4) partial coordination number (larger particles to larger particles), and 5) partial coordination number (smaller particles to smaller particles). The purpose of these coordination numbers was to determine which of these parameters, if any, was related to the overall packing density. In the examples that follow, results of these five values are shown with regard to the different disruptor geometries. The patterns of change in these five parameters are different. A working hypothesis of this thesis is that the larger coordination number of the larger particles leads to a prediction of a larger packing density.

Table 2: Mean coordination number and partial coordination number of particles

Model	A(0)	B(50)	C(47.1)	D(97.1)	E(97.1)	F(147.1)
All	3.701	3.740	3.766	3.880	3.902	3.846
Larger	6.787	6.906	6.785	7.023	7.199	7.158
Smaller	2.673	2.685	2.750	2.833	2.804	2.742
Larger to Larger	4.652	4.618	4.562	4.590	4.622	4.067
Smaller to Smaller	2.306	2.337	2.414	2.427	2.322	2.295

As shown in Table 2, the maximum value of the mean coordination number of all particles is obtained from Model E. Model E also yields the maximum value of coordination number of larger particles in this group. Model D gives the maximum value of the mean coordination number of smaller particles, but this value is only 1 percentage larger than the value in Model

E. The value of Model E is still relatively large in group of coordination number of smaller particles. The maximum value of partial coordination number is also obtained from Model E.

In the group (Model A, B, D, F), the mean coordination number does not always increase with the complexity of geometry. With increasing complexity of disruptor geometry, the mean coordination number of all the particles generally increases. The only exception is Model F. This configuration has the most complicated geometry in the group, which implies that the motion of particles is the most complicated. However, the mean coordination number for this system decreases 0.8 and 3.1 percentage in comparison to Model D. The mean coordination number of the larger particles does increase gradually with complexity of system geometry.

In general, the mean coordination number increases as disruptors complexity increases in complexity in the group (Model A, C, E). Model C has only one semi-circle shape disruptor that forces the particles to flow towards the two sides. This disruptor has a negligible influence on the coordination number for the larger particles. Model E includes only one semi-circular shape disruptor and one pair of edge disruptors along the wall at bottom of the disruptor that forces the particles to flow towards the center line of the disruptor. The wall disruptor causes a 6.1% increase in the coordination number of larger particles (Model A, C, E). In the group of result (Model A, C, D), the mean coordination number increases as disruptors complexity increases in complexity.

The mean coordination number for larger particles increases when the general complexity of the geometry of the disruptors increases. The mean coordination number of all the particles and smaller particle have a similar pattern but do not always increase with complexity of geometry of disruptor.

4.2 Mean vertical position of smaller particles

In the present simulation with the ratio of radii of the two particle types given as 5, most of the smaller particles settle at the bottom of container as shown in Figure 32. The final vertical position of the smaller particles slightly changes with the complexity of geometry of the disruptors. The mean vertical positions of the smaller particles in each model was also measured to determine if there was a relationship between this variable and other parameters such as local and global packing density.

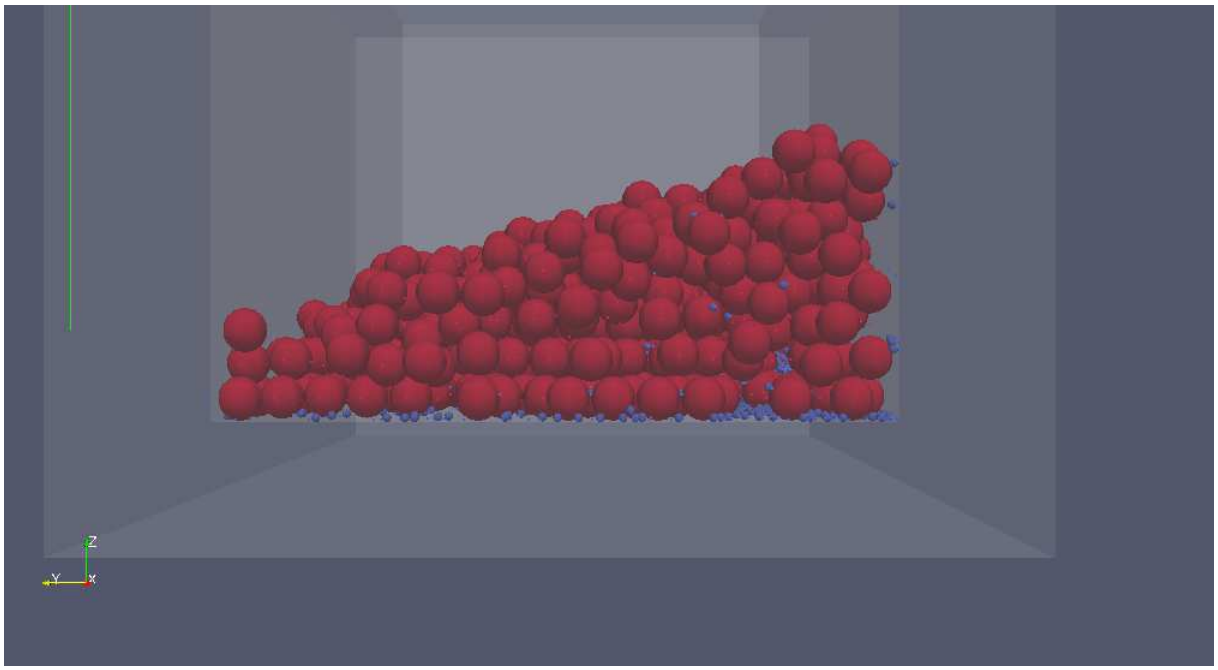

Figure 32: Side view of the container

Table 3: Mean vertical position of smaller particles

Model	A(0)	B(50)	C(47.1)	D(97.1)	E(97.1)	F(147.1)
Smaller	0.1358	0.1329	0.1309	0.1312	0.1284	0.1271

The smaller particles in Model F had the lowest mean vertical position, and the smaller particles in Model A had highest mean vertical position. This validates that the more complex mixing results in more small particles located on the bottom of the packing. In the

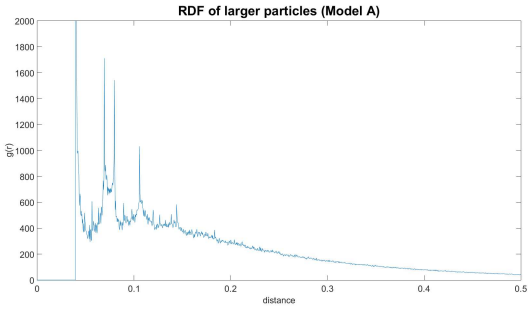

Figure 33: RDF of larger particle (A)

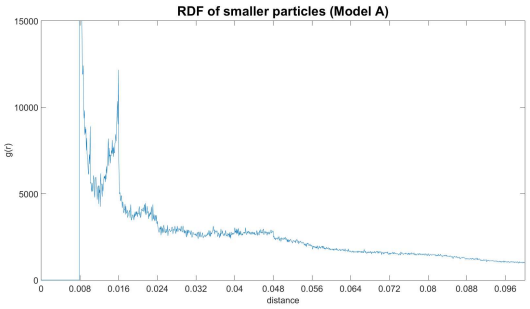

Figure 34: RDF of smaller particle (A)

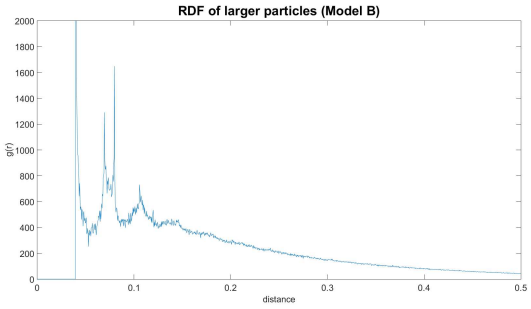

Figure 35: RDF of larger particle (B)

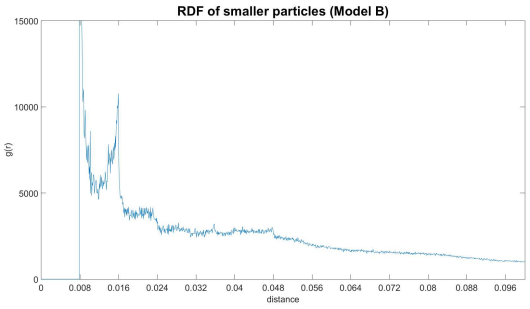

Figure 36: RDF of smaller particle (B)

following tables, this parameter is shown in order of complexity of geometry of mixer.

In conclusion, mean vertical position of smaller particle decrease when the complexity of geometry increase.

4.3 Radial distribution function

There are very few studies of particle packings that use the radial distribution function of bidisperse spheres, with the work of Isola (2008) [19] being the only exception found by the author. The method developed by Isola (2008) [19] is used in this thesis to study the RDF of bidisperse packings. The radial distribution function is calculated and plotted separately for larger and smaller particles for the simulations modeled in this study. The RDF plot of larger and smaller particles were compared to RDF plots of mono-size packings, which is a well understood behavior based on numerous studies completed in the past few decades.

In all radial distribution functions of the larger particles computed for this study, the first splitting of the second peak can be observed. This means that the packing of the larger

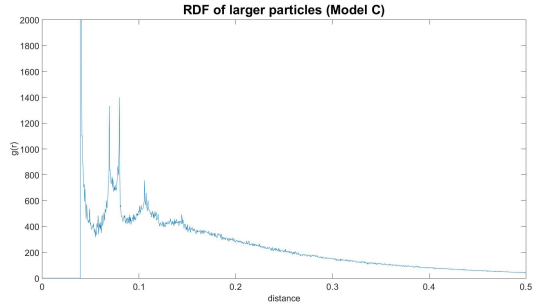

Figure 37: RDF of larger particle (C)

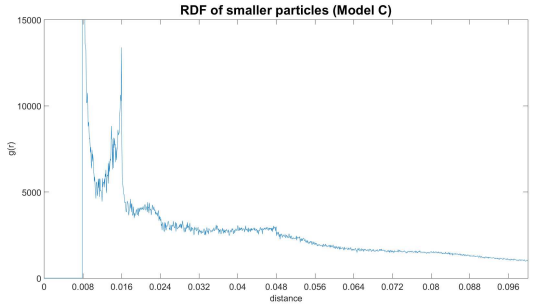

Figure 38: RDF of smaller particle (C)

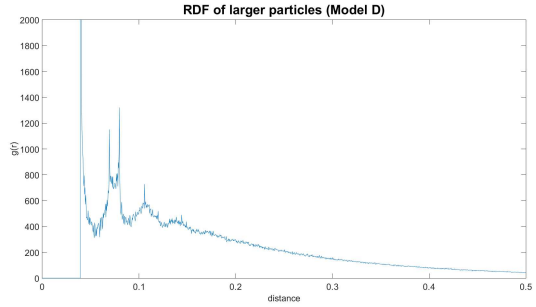

Figure 39: RDF of larger particle (D)

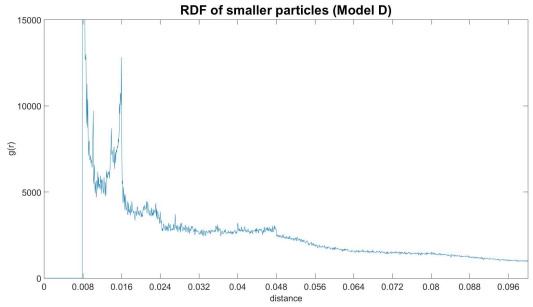

Figure 40: RDF of smaller particle (D)

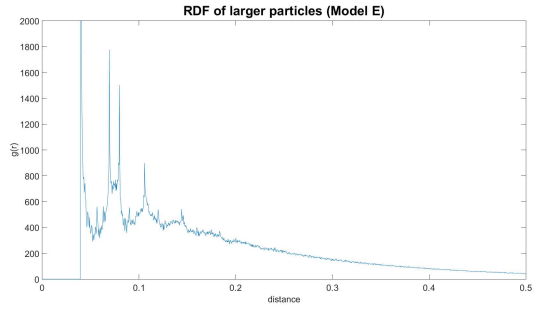

Figure 41: RDF of larger particle (E)

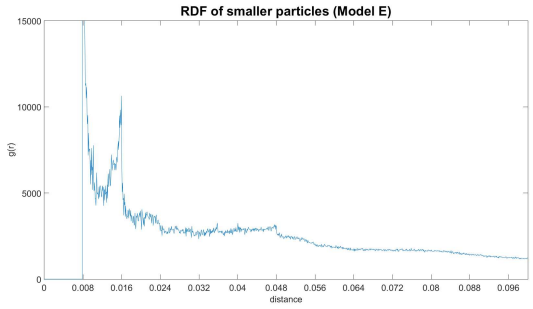

Figure 42: RDF of smaller particle (E)

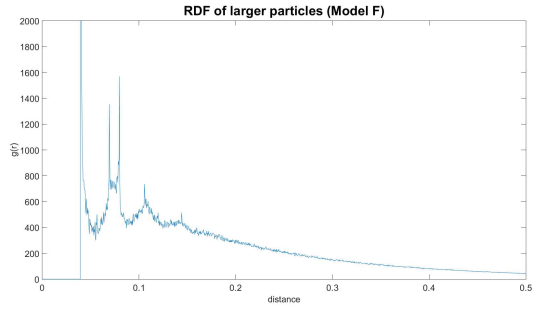

Figure 43: RDF of larger particle (F)

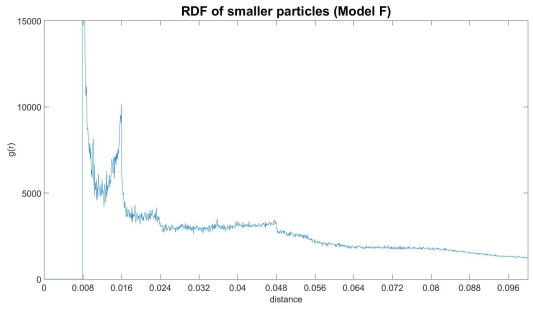

Figure 44: RDF of smaller particle (F)

particles in all of the models is representative of a dense packing. The presence of the third peak is visible at distance around 3d. The fourth peak begins to be visible at a distance of around 4d. Since the same mixture ratio is used in each model, the larger spheres dominate packing structure. According to Isola (2008) [19], the characteristics of the RDF for each size of particle in binary mixtures is identical to those that appear for mono-size particle packings.

According to the behavior of the radial distribution function of the smaller particles, the overall packing of the smaller particles is less dense than the packing of the larger particles. This is because the second splitting of the second peak is not sharp in the radial distribution function of the smaller particles.

In conclusion, the radial distribution function of each type of particle in a binary mixture has the same characteristics of radial distribution function of mono-size particle packing. The first splitting of the second peak in the radial distribution function of larger particles vanishes when the global packing density decreases. The second splitting of the second peak in radial distribution function of the smaller particles vanishes when the local packing density of the smaller particles decreases.

4.4 Packing density

4.4.1 Global packing density

The global packing density was calculated for each of the final packings. The magnitude of the global packing density may be slightly influence by the control volume used based on the location of the center of the particles. The global packing densities of the models are obtained using the same method so the relative magnitude of the global packing density is consistent.

Table 4: Control volume and global packing density

Model	Control volume	Global packing density
A (0)	0.1093	0.6232
B (50)	0.1107	0.6193
C (47.1)	0.1096	0.6258
D (97.1)	0.1109	0.6188
E (97.1)	0.1076	0.6374
F (147.1)	0.1099	0.6244

Table 5: Global packing density and mean coordination number of all the particles (the value of mean coordination number increase from top to bottom)

Model	Global PD	percent increase	CN of all the particles	percent increase
A	0.6232		3.7015	
B	0.6193	-0.6%	3.7405	1%
C	0.6258	1%	3.766	0.6%
F	0.6244	-0.2%	3.8465	1%
D	0.6188	-0.8%	3.8809	0.8%
E	0.6374	3%	3.9028	0.5%

Table 6: Global packing density and mean coordination number of larger particles (the value of mean coordination number increase from top to bottom)

Model	Global PD	percent increase	CN of larger particles	percent increase
C	0.6258		6.785	
A	0.6232	-0.4%	6.787	0.02%
B	0.6193	-0.6%	6.9065	1.7%
D	0.6188	-0.08%	7.023	1.6%
F	0.6244	0.9%	7.1580	1.9%
E	0.6374	2%	7.1990	0.5%

Table 7: Global packing density and mean coordination number of smaller particles (the value of mean coordination number increase from top to bottom)

Model	Global PD	percent increase	CN of smaller particles	percent increase
A	0.6232		2.6730	
B	0.6193	-0.6%	2.6852	0.1%
F	0.6244	1%	2.7427	2%
C	0.6258	-0.2%	2.75	0.2%
E	0.6374	-0.8%	2.8040	1.9%
D	0.6188	3%	2.833	1%

Table 8: Global packing density and mean partial coordination number (Larger to Larger) (the value of mean coordination number increase from top to bottom)

Model	Global PD	percent increase	partial CN	percent increase
F	0.6244		4.067	
C	0.6258	0.2%	4.562	12%
D	0.6188	-1%	4.590	0.6%
B	0.6193	0.08%	4.618	0.6%
E	0.6374	2.9%	4.622	0.08%
A	0.6232	-2.2%	4.652	0.64%

Table 9: Global packing density and mean partial coordination number (Smaller to Smaller) (the value of mean coordination number increase from top to bottom)

Model	Global PD	percent increase	partial CN	percent increase
F	0.6244		2.295	
A	0.6232	-0.1%	2.306	4.7%
E	0.6374	2.2%	2.322	0.6%
B	0.6193	-2.8%	2.337	0.6%
C	0.6258	1%	2.414	3.2%
D	0.6188	-1.1%	2.427	0.5%

According to Table 4, maximum value of global packing density is Model E, which is three percent higher than the packing with the lowest density. According to Beck (2003) [28], there is linear relationship between partial coordination number and global packing density for binary mixture. But this theory is only true under the packing structure is gapless. As shown in Table 5 to 9, the global packing density does not increase with the mean coordination number and mean partial coordination number.

Result in the order of the complexity of disruptor

As discussed in the result of the mean coordination number part, the mean coordination number almost always increase with the complexity of geometry of disruptor. For the mono-size particle packing, the coordination number always increase with global packing density. To determine the relationship between the coordination number and the global packing density of binary mixtures, the relationship between the coordination number and the global packing density was examined. A careful analysis was completed that compared the global packing density to the various coordination number presented in earlier sections. The only significant finding was that global packing density increases with the mean coordination number of all the particle, larger particles and smaller particles in the group (Model A, C, E).

Table 10: Global packing density and mean coordination number of smaller particles (the complexity of geometry of disruptor increase from top to bottom)

Model	Global PD	percent increase	CN of smaller particles	percent increase
A	0.6232		2.6730	
C	0.6258	0.4%	2.75	2.8%
E	0.6374	1.8%	2.8040	1.9%

Table 11: Global packing density and mean coordination number of lager particles (the complexity of geometry of disruptor increase from top to bottom)

Model	Global PD	percent increase	CN of larger particles	percent increase
A	0.6232		6.787	
C	0.6258	0.4%	6.785	-0.029%
E	0.6374	1.8%	7.199	6.1%

Table 12: Global packing density and mean coordination number of all the particles (the complexity of geometry of disruptor increase from top to bottom)

Model	Global PD	percent increase	CN of all the particles	percent increase
A	0.6232		3.7015	
C	0.6258	0.4%	3.766	1.7%
E	0.6374	1.8%	3.9028	3.6%

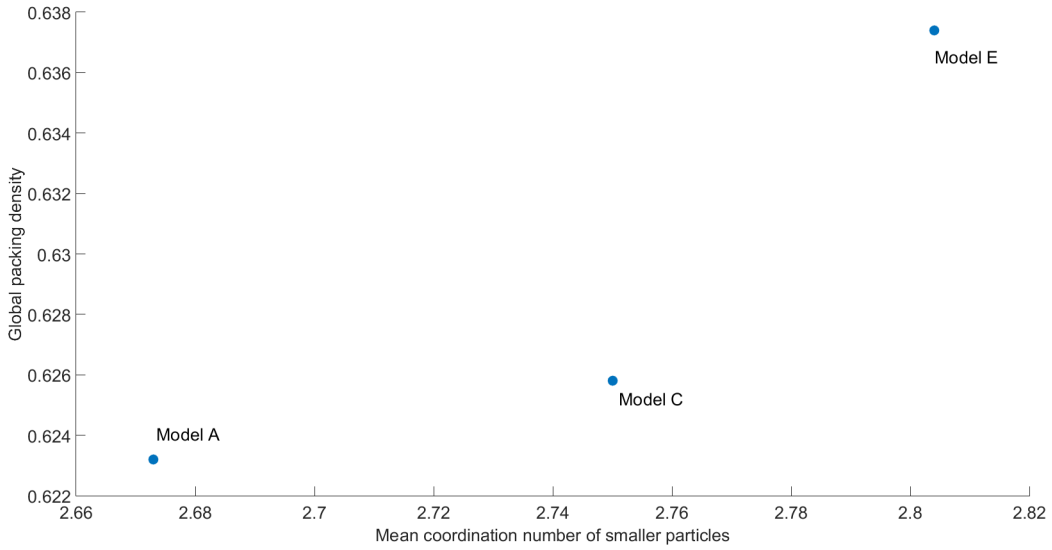

Figure 45: The relationship between the global packing density and the mean coordination number of smaller particles

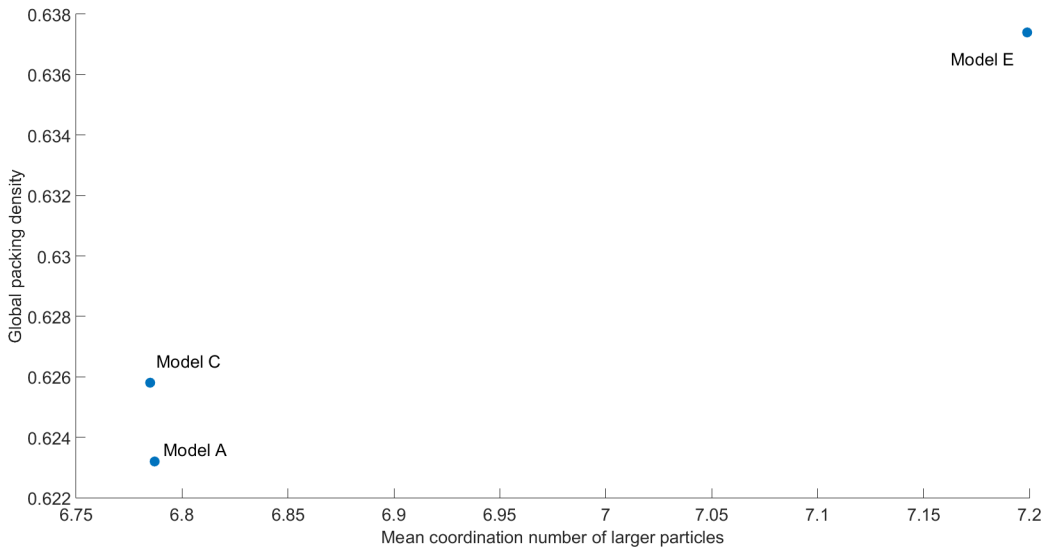

Figure 46: The relationship between the global packing density and the mean coordination number of larger particles

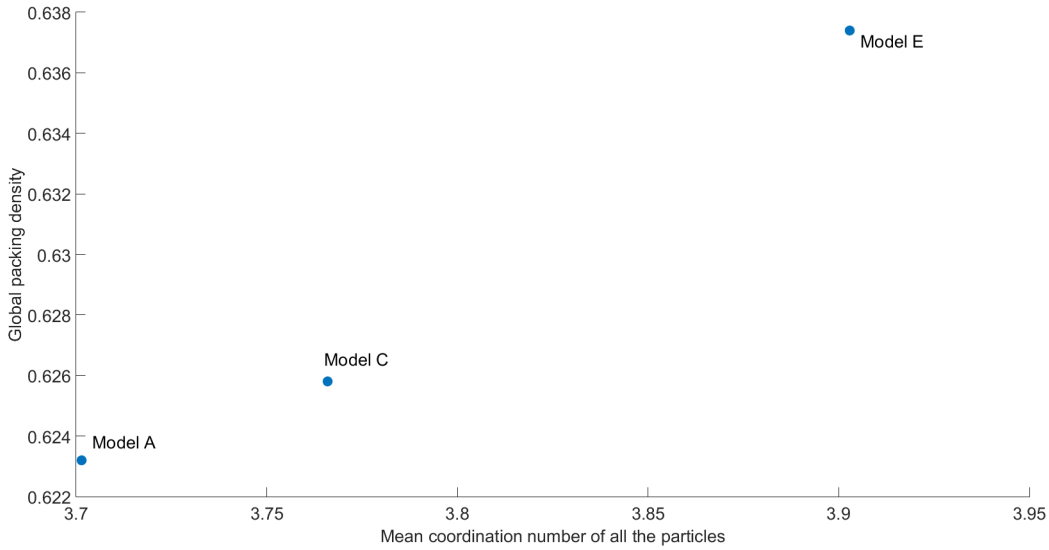

Figure 47: The relationship between the global packing density and the mean coordination number of all the particles

4.4.2 Local packing density

In the present model, the radical Voronoi tessellations are calculated by the algorithm Voro++. Voro++ is an open source software library for the computation of the Voronoi diagram. Because of the time constraints, particles are only able to fill the half of container. The particles at the top surface were eliminated since the boundary used to calculate radical tessellation is set to the boundary of container. Frequency histograms of the volume of the radical tessellations were used to find the volumes of the radical tessellation of particles at the top surface of the packing.

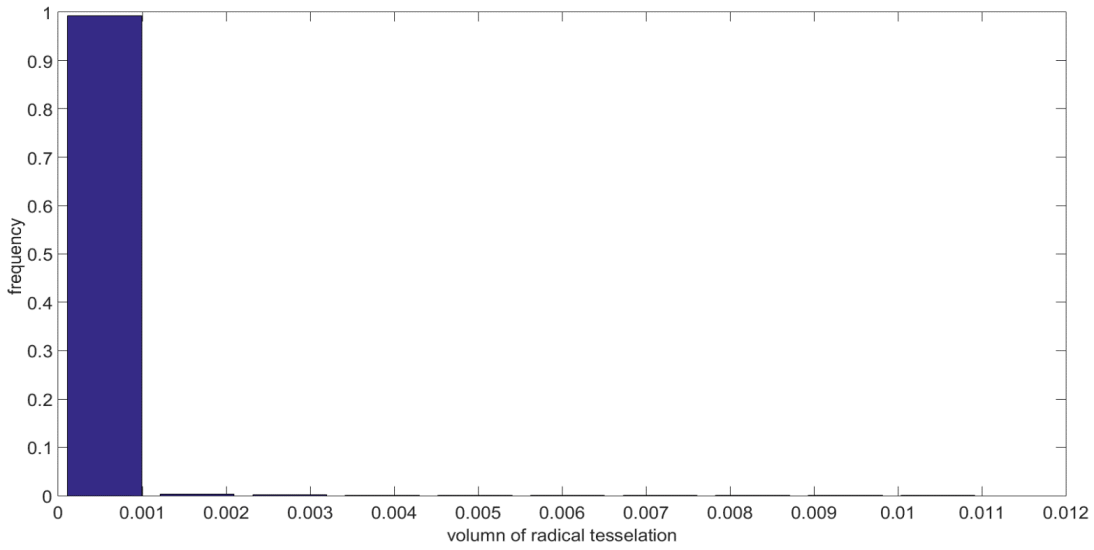

Figure 48: Frequency histograms of volume of radical tessellation of model A

The top boundary of radical tessellation is set to the top boundary of container, and the particles in six models only fill half the container. Almost all the volume of the radical tessellation from model A is less than 0.001 m^3 so the volume which is larger than 0.001 m^3 is highly possible to be volume of radical tessellation of particle at top surface of packing. The result of all the volume of radical tessellation from other models share the same pattern with model A. So all the volume that is larger than 0.001 m^3 are eliminated from calculating mean volume of radical tessellation and mean local packing density. The results of the mean radical tessellation and mean local packing density are shown in Tables 13 and Table 14.

Table 13: Mean volume of radical tessellation of all the particle

Model	Mean volume of radical tessellation
A	1.917e-05
B	1.938e-05
C	1.943e-05
D	1.978e-05
E	1.951e-05
F	1.946e-05

As shown in Table 13, the maximum value of the mean volume of the radical tessellation of all the particles is Model D.

Table 14: Mean local packing densities

Model	Larger	Smaller	all
A	0.5959	0.3262	0.3914
B	0.5951	0.3290	0.3937
C	0.5896	0.3351	0.3970
D	0.5870	0.3319	0.3940
E	0.5959	0.3262	0.3922
F	0.5888	0.3268	0.3907

From Table 14, the maximum value of the mean local packing density of the larger particles is Model A and Model E. The maximum value of the mean local packing density of the smaller particles is Model C. The maximum value of mean local packing density of all the particles is Model C. After a analysis of relationship of coordination number and local packing density, no connection is found between these two parameters.

5 CONCLUSION

The primary conclusions of this work can be summarized as follow for binary mixing of particles:

1. The mean coordination number of all particles generally increases with the complexity of the geometry of disruptor.

2. The mean coordination number of larger particles generally increases with the complexity of geometry of disruptor.

3. The mean coordination number of smaller particles generally increases with the complexity of geometry of disruptor.

4. The partial mean coordination number (larger to larger and smaller to smaller) does not increase with the complexity of geometry of disruptor.

5. The mean vertical position of smaller particles, this parameter decreases with a increase in the complexity of the geometry of the disruptor.

6. The radial distribution function of each type of particle in a binary mixture has the same characteristics of radial distribution function of mono-size particle packing.

7. The first splitting of the second peak in the radial distribution function of larger particles vanishes when the global packing density decreases.

8. The second splitting of the second peak in radial distribution function of the smaller particles vanishes when the local packing density of the smaller particles decreases.

9. In the present result, there is no linear relationship between partial coordination number and global packing density.

10. No linear relationship was found between the coordination number and the global packing density.

11. Neither coordination number nor partial coordination number have linear relationships with the local packing density and the mean volume of the radical tessellation.

REFERENCES

[1] ZP Zhang, LF Liu, YD Yuan, and AB Yu. A simulation study of the effects of dynamic variables on the packing of spheres. *Powder Technology*, 116(1):23–32, 2001.

[2] HP Zhu, ZY Zhou, RY Yang, and AB Yu. Discrete particle simulation of particulate systems: theoretical developments. *Chemical Engineering Science*, 62(13):3378–3396, 2007.

[3] Benjamin E Wickland, G Ward Wilson, Dharma Wijewickreme, and Bern Klein. Design and evaluation of mixtures of mine waste rock and tailings. *Canadian Geotechnical Journal*, 43(9):928–945, 2006.

[4] Jacques Duran. *Sands, powders, and grains: an introduction to the physics of granular materials*. Springer Science & Business Media, 2012.

[5] Peter A Cundall and Otto DL Strack. A discrete numerical model for granular assemblies. *Geotechnique*, 29(1):47–65, 1979.

[6] PETER A Cundall and ODL Strack. The development of constitutive laws for soil using the distinct element method. *Numerical methods in geomechanics*, 1:289–317, 1979.

[7] HC Hamaker. The londonvan der waals attraction between spherical particles. *physica*, 4(10):1058–1072, 1937.

[8] Jacob N Israelachvili. *Intermolecular and surface forces: revised third edition*. Academic press, 2011.

[9] Godehard Sutmann. *Classical molecular dynamics*, volume 10. Citeseer, 2002.

[10] Heinrich Hertz. Über die berührung fester elastischer körper. *Journal für die reine und angewandte Mathematik*, 92:156–171, 1882.

[11] Marc Lätzel, Stefan Luding, and Hans J Herrmann. Macroscopic material properties from quasi-static, microscopic simulations of a two-dimensional shear-cell. *Granular Matter*, 2(3):123–135, 2000.

[12] PA Langston, U Tüzün, and DM Heyes. Continuous potential discrete particle simulations of stress and velocity fields in hoppers: transition from fluid to granular flow. *Chemical Engineering Science*, 49(8):1259–1275, 1994.

[13] H. Deresiewicz R.D. Mindlin. Elastic spheres in contact under varying oblique forces. *Journal of Applied Mechanics*, (20):327–344, 1953.

[14] Otis R Walton and Robert L Braun. Viscosity, granular-temperature, and stress calculations for shearing assemblies of inelastic, frictional disks. *Journal of Rheology (1978-present)*, 30(5):949–980, 1986.

[15] Yutaka Tsuji, Toshihiro Kawaguchi, and Toshitsugu Tanaka. Discrete particle simulation of two-dimensional fluidized bed. *Powder technology*, 77(1):79–87, 1993.

[16] BH Xu and AB Yu. Numerical simulation of the gas-solid flow in a fluidized bed by combining discrete particle method with computational fluid dynamics. *Chemical Engineering Science*, 52(16):2785–2809, 1997.

[17] HP Zhu, ZY Zhou, RY Yang, and AB Yu. Discrete particle simulation of particulate systems: a review of major applications and findings. *Chemical Engineering Science*, 63(23):5728–5770, 2008.

[18] Leonardo E Silbert, Deniz Ertaş, Gary S Grest, Thomas C Halsey, and Dov Levine. Geometry of frictionless and frictional sphere packings. *Physical Review E*, 65(3):031304, 2002.

[19] Riccardo Isola. *Packing of granular materials*. University of Nottingham, 2008.

[20] Tomaso Aste, Mohammad Saadatfar, and TJ Senden. Geometrical structure of disordered sphere packings. *Physical Review E*, 71(6):061302, 2005.

[21] Catherine OSullivan. *Particulate Discrete Element Modelling: A Geomechanics Perspective. Applied Geotechnics*. Spon Press/Taylor & Francis, 2011.

[22] Christoph Kloss, Christoph Goniva, Alice Hager, Stefan Amberger, and Stefan Pirker. Models, algorithms and validation for opensource dem and cfd–dem. *Progress in Computational Fluid Dynamics, an International Journal*, 12(2-3):140–152, 2012.

[23] Alberto Di Renzo and Francesco Paolo Di Maio. Comparison of contact-force models for the simulation of collisions in dem-based granular flow codes. *Chemical engineering science*, 59(3):525–541, 2004.

[24] JC Macrae and WA Gray. Significance of the properties of materials in the packing of real spherical particles. *British Journal of Applied Physics*, 12(4):164, 1961.

[25] John-Paul Latham, Ante Munjiza, and Yang Lu. On the prediction of void porosity and packing of rock particulates. *Powder Technology*, 125(1):10–27, 2002.

[26] RY Yang, RP Zou, and AB Yu. Effect of material properties on the packing of fine particles. *Journal of applied physics*, 94(5):3025–3034, 2003.

[27] Louis Caryl Graton and HJ Fraser. Systematic packing of spheres: with particular relation to porosity and permeability. *The Journal of Geology*, pages 785–909, 1935.

[28] JM Beck and VA Volpert. Gapped gapless packing structures. *Journal of colloid and interface science*, 262(1):162–170, 2003.

6 APPENDIX

In this Appendix,a brief review of other particle models is presented to assist further research.

6.1 Packing of cohesionless particle

Force network : Force network from DEM simulation show good agreement with physical experiment (Silbert et al., 2002b; Snoeijer et al., 2003). In earlier study, physical experiment had been developed to study force network of particle parking. The probability density function is used to show force distribution. A feature of probability density function of monosized particle has been found by Brujic (2003), PDF has an exponential tail when the force is larger than only one particle weight. This feature is also observed in DEM simulation.

6.2 Particle flow

In this area, the researchers mainly focused on two aspects: fundamental and applied. Fundamental research is that simplified system is used to understand basic characteristic of particle flow. Goal of applied research is modeling the manufacturing process in practice with DEM.

6.2.1 Fundamental research

Simple geometric is used in fundamental research to simplified problem. The result from fundamental research is general which is applicable to different areas. In fundamental research, two different kinds of particle flow (confined flow and non-confined flow) were studied.

Confined flow: The definition of confined flow is that boundary of a flow are confined. Earlier research about confined flow is mainly based on physical experiment. The results from these physical experiments usually are used to support continuum theories. But these results are useless for understanding the microscopic characteristics of granular material

since detail of internal structure of particle flow is difficult to gain. With development of DEM simulation, many researchers started to simulate confined flow by discrete element method. And results from physical experiment and DEM simulation are compared to validate accuracy of DEM. Different shearing flows were studied such as direct shear, vertical flow, triaxial compression. Unconfined flow:Unconfined flow is the particle flow that at least one of its sides is unconfined.

6.2.2 Applied research

The aim of applied research is modeling operation in practice by DEM to figure out the particle dynamic in this area. The behavior of particle flow is highly depended on interaction between device and particle. In earlier research, many researchers were trying to understand particle behavior by photographic experiment which is lack of detail of particle system. And lots of non-invasive experimental techniques were developed such as positron emission particle tracking (PEPT) (Broadbent et al., 1995; Parker et al., 1997; Stewart et al., 2001) and magnetic resonance imaging (MRI) (Nakagawa et al., 1993; Sederman et al., 2007). But these experiments also have some shortcomings such high cost, no detail of interaction force between particles. The limitation of experiment makes DEM important for simulating particle systems.

Flow in hoppers:

Hopper is a device which is geometrical simple and widely used. In past decade, flow in hopper has been studied by various researchers from experimental and numerical. Different hopper geometers were modelled including two-dimensional model (Langston et al., 1994, 1995a,b, 1997, 2004; Ristow and Herrmann, 1995; Kohring et al., 1995; Rong, 1995a,b; Potapov and Campbell, 1996; Ristow, 1997; Rotter et al., 1998; Holst et al., 1999b; Masson and Martinez, 2000a,b; Favier et al., 2001; Sanad et al., 2001; Cleary and Sawley, 2002; Wassgren et al., 2002; Fraige and Langston, 2004; Parisi et al., 2004), and three-dimensional model (Sakaguchi et al., 1993; Hidaka et al., 1994; Yuu and Umekage, 1995; Yuu et al., 1995;

Langston et al., 1995a,b, 1996, 1997, 2004; Lu et al., 1997; Negi et al., 1997; Kano et al., 1998; Gutfraind and Savage, 1998; Umekage et al., 1998; Baxter et al., 2000; Joseph et al., 2000; Hirshfeld and Rapaport, 2001; Xu et al., 2002b; Zhu and Yu, 2001, 2004, 2005a,b; Theuerkauf et al., 2003; Tuzun et al., 2004; Li et al., 2004b; Lia et al., 2004; Abou-Chakra et al., 2004; Goda and Ebert, 2005; Zhu et al., 2005, 2006; Balevicius et al., 2006, 2007, 2008; Kruggel-Emden et al., 2006; Ketterhagen et al., 2007, 2008; Datta et al., 2008).

In modeling and experiment, the results are mainly focus on wall stress/pressure, discharge rate and internal properties since these three values are essential for hopper design. In order to validate applicability of discrete element method for particle flow in hopper, many researchers compare the result from experiment with numerical analysis. And they find two results match (Langston et al., 1995a; Negi et al., 1997; Holst et al., 1999a,b; Rotter et al., 1998; Masson and Martinez, 2000a,b; Goda and Ebert, 2005).

Several common variables were used which are geometer of hopper, material properties and flow condition. Cleary and Sawley (2002) mentioned that particle shape is also a variable since it has good influence on wall pressure. Langston (1996) proposed that air-assisted flow causes larger wall pressure so it can not be ignored in hopper design. Discharge rate is essential to be predicted since it is assisted with control of transport system. But it is complex due to various variables such as particle characteristic and material properties. Discrete element method can solve this problem. And its result matches the result from experiment (Langston et al., 1994, 1995a; Kano et al., 1998; Zhu and Yu, 2004). Some unimportance variables were successfully eliminated and important variables have been found. The result from DEM simulation states that discharge rate is strongly concerned to particle friction, however, stiffness of particle, wall roughness and damping ratio has small influence on discharge rate (Langston et al., 1994, 1995a; Kano et al., 1998; Zhu and Yu, 2004). Hopper geometer and operation also can affect discharge rate (Langston et al., 1994, 1995a; Kano et al., 1998; Zhu and Yu, 2004).

The force network, internal structure of particle flow, particle behavior is three important proprieties. In earlier study, these proprieties are difficult to gain from experiment. However, DEM simulation is focus on every individual particle in system. Due to This characteristic these proprieties are easy to gain from DEM simulation. The study related to this area is mainly focused on two aspects:

Special distributions: according to different flow pattern, flow structure and force structure, particle flow in hopper have few flow zones as shown in figure 21(Langston et al., 1994, 1995b, 1996; Rong et al., 1995a,b; Rotter et al., 1998; Parisi et al., 2004). Zhu and Yu (2004) mentioned that particle flow in a cylindrical hopper has four different flow zone which are stagnant, plug flow, converging flow and transitional zone.

Statistical distribution: Common statistical distributions of the properties in DEM simulation usually include velocity of each individual particle, coordination number, porosity and force network. And these statistical distribution can also be used to describe the effect of particle properties and hopper geometer quantitatively (Zhu and Yu, 2004).

Flow in disruptors:

disruptors is a common and widely used device in many industries. It is essential to understand behavior of particle flow when particles are mixing. Inadequate mixing is possible to lead to bad result so effect factors on particle mixing are necessary to be figured out. Common effect factors of particle mixing have geometry of disruptors, particle properties. Various disruptorss have been studied such as rotational disruptors (Moakher et al., 2000; Kuo et al., 2002; Lemieux et al., 2007, 2008; Sudah et al., 2005; Arratia et al., 2006; Moakher et al., 2000), external surface driven disruptors (Endoh et al., 2000; Iwasaki et al., 2001; Hotta et al., 2001; Kano et al., 2001), internal blade driven disruptors (Gyenis et al., 1999; Kaneko et al., 2000; Schutyser et al., 2003; Stewart et al., 2001; Terashita et al., 2002; Zhou et al., 2003c, 2004d; Kuo et al., 2004; Spillmann et al., 2005; Bertrand et al. 2005; Sato et al., 2008; Muguruma et al., 1997; Chaudhuri et al., 2006; Chen et al., 2004).

To prove validity of discrete element method, various experiments have been conducted. And measured results have a good agreement with numerical results in different way.

Visual comparison of flow pattern: as show in Figure 49, Moakher et al. (2000) mentioned that experimental result of double-cone and v-blender match numerical result.

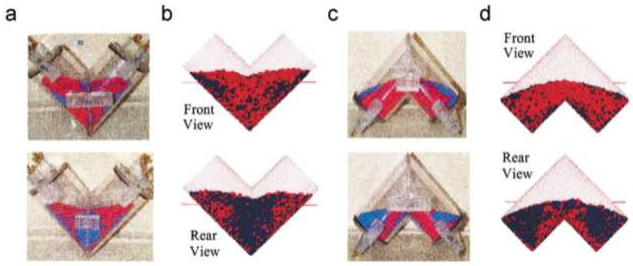

Figure 49: Patterns from (a) experiment with different size particles in upright transparent V-blender; (b) corresponding simulation after two revolutions; (c) experiment in inverted orientation; and (d) simulation in inverted orientation (Moakher et al., 2000).

Particle scale comparison: PEPT experiment is used to get experimental result. Vertical bladed disruptor, conical helical-disruptor and V-blender have been studied (Stewart et al., 2001; Schutyser et al., 2003; Kuo et al., 2002). As shown in Figure 50, measured results match numerical result.

Due to the complexity of disruptor motion, particle motion in different disruptor have totally different pattern. Helical disruptor (Schutyser et al., 2003), vertical axis bladed disruptor (Zhou et al., 2003c, 2004d), tote blender (Arratia et al., 2006), double-cone blender and V-blender (Moakher et al. 2000) have been studied to understand the motion of particle in these disruptors.

The studies of particle flow in disruptor are mainly focused on method that can be used to optimize the performance of a disruptor. DEM simulation can perfectly solve this problem since mixing can be quantified at any mixing stage. Muguruma et al. (1997) mentioned that particle flow in rotating mixing is possible to be mixed better by using baffle with optimal length/height ratio. Zhou et al. (2003c) proposed that mixing performance of any mixing can be optimized by reducing the difference in particle size or density. Sudah et al. (2005) show that better axial mixing rates could be achieved by axial offset, installing a hopper or

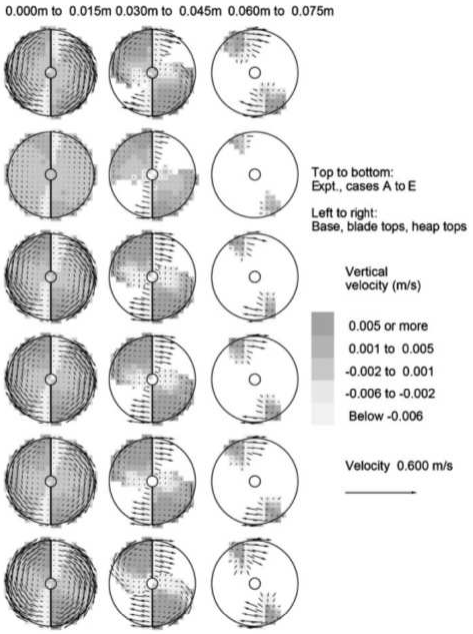

Figure 50: Velocity fields of a bladed disruptor at different heights from PEPT experiment and DEM simulations. The top layer represents the experimental results, while others are the simulated results for five cases with different sliding and rolling friction coefficients: case A, 0.2 and 0.025 mm; case B, 0.3 and 0.0 mm; case C, 0.3 and 0.025 mm; case D, 0.3 and 0.05 mm; case E, 0.5 and 0.025 mm. The cell shade indicates the vertical velocity while the vectors show horizontal velocity (Stewart et al., 2001).

bin section in tote blender.

Particle flow in drums and mill:

Due to the motion of rotating drums and mill, particle flow have complex pattern in these devices. Rotating drums and mill is two common device in industry such as chemistry, civil engineering. It is necessary to figure out dynamic behavior of particle flow in these devices. Thus various method of tracking particle motion has been developed in past two decades. PEPT (Broadbent et al., 1995; Parker et al., 1997) and MRI (Nakagawa et al., 1993) are two common experimental techniques to study particle behavior in the system. With development of DEM, it turn out to be useful numerical method to simulate particle flow in rotating drums and mills. Measured result and numerical result have been compared to validate DEM (Yamane et al., 1998; Yamane, 2001; Yamane et al., 1998; Yamane, 2001; Yang et al., 2003b; Yamane, 200; Yang et al., 2003b). DEM can overcome some limitation

of experimental techniques such as lack of detail of internal information of particle flow. Particle flows in various devices have been simulated by DEM:

1. Drum mainly the horizontally rotating drums.
2. Mill including tumbling ball mill.